

# Spectral features of tidal-disruption candidates and alternative origins for such transient flares

Curtis J. Saxton<sup>\*</sup>, Hagai B. Perets & Alexei Baskin

*Physics department, Technion - Israel institute of Technology, Haifa, Israel 3200002*

Accepted —. Received —; in original form —

## ABSTRACT

UV and optically selected candidates for stellar tidal disruption events (TDE) often exhibit broad spectral features (He II emission, H $\alpha$  emission, or absorption lines) on a blackbody-like continuum ( $10^4\text{K} \lesssim T \lesssim 10^5\text{K}$ ). The lines presumably emit from TDE debris or circumnuclear clouds photoionized by the flare. Line velocities however are much lower than expected from a stellar disruption by supermassive black hole (SMBH), and are somewhat faster than expected for the broad line region (BLR) clouds of a persistently active galactic nucleus (AGN). The distinctive spectral states are not strongly related to observed luminosity and velocity, nor to SMBH mass estimates. We use exhaustive photoionization modelling to map the domain of fluxes and cloud properties that yield (e.g.) a He-overbright state where a large He II(4686Å)/H $\alpha$  line-ratio creates an illusion of helium enrichment. Although observed line ratios occur in a plausible minority of cases, AGN-like illumination can not reproduce the observed equivalent widths. We therefore propose to explain these properties by a light-echo photoionization model: the initial flash of a hot blackbody (detonation) excites BLR clouds, which are then seen superimposed on continuum from a later, expanded, cooled stage of the central luminous source. The implied cloud mass is substellar, which may be inconsistent with a TDE. Given these and other inconsistencies with TDE models (e.g. host-galaxies distribution) we suggest to also consider alternative origins for these nuclear flares, which we briefly discuss (e.g. nuclear supernovae and starved/subluminous AGNs).

**Key words:** accretion, accretion discs — black hole physics — galaxies: active — galaxies: nuclei — quasars: emission lines

## 1 INTRODUCTION

Early theorists considered that active galactic nuclei (AGN) and quasars might consist of a supermassive black hole (SMBH, of mass  $m_\bullet$ ) accreting gas derived from the tidal disruption of stars in the nuclear cluster (Hills 1975; Frank & Rees 1976; Young, Shields & Wheeler 1977; Ozernoi & Reinhardt 1978; Kato & Hōshi 1978). A star of mass  $m_\star$  and radius  $R_\star$  disrupts if it passes within the ‘tidal radius,’  $R_t = R_\star(m_\bullet/m_\star)^{1/3}$ . The consequences would be similar if the nucleus hosts any other sufficiently dense and relativistic type of dark supermassive object (e.g. Goel et al. 2015; Meliani et al. 2015; Saxton, Younsi & Wu 2016). Larger SMBH ( $m_\bullet \gtrsim \text{few} \times 10^8 m_\odot$ ) can swallow main sequence stars whole, without a tidal disruption event (TDE). The TDE rate needed to power AGN

turned out to be difficult to reconcile with stellar densities, at least in the nuclei of modern galaxies (and gas accretion now seems more important to AGN). Nonetheless it was recognized that a TDE could produce a distinctive flare, peaking in much less than a year and potentially remaining observable during a few years of fading (Lidskii & Ozernoi 1979; Gurzadian & Ozernoi 1981; Lacy, Townes & Hollenbach 1982; Luminet & Marck 1985; Rees 1988). TDEs by lower mass SMBHs ( $m_\bullet \lesssim 3 \times 10^7 m_\odot$ ) are more likely to accrete at rates exceeding the Eddington (1918) radiation pressure limit (Ulmer 1999).

More than ten transient events detected in ultraviolet and optical (UV/O), X-ray and  $\gamma$ -ray monitoring and serendipitous observations are currently classified as TDE candidates (Komossa 2015). These were selected for their central locations in the host galaxies. Candidates are usually excluded if the host showed conventional signatures of an AGN (in spectroscopy, variability, and radio counterparts)

<sup>\*</sup> E-mail: saxton@physics.technion.ac.il (CJS); hperets@physics.technion.ac.il (HBP); alexei@physics.technion.ac.il (AB).

before and long after the transient<sup>1</sup>. The relation between TDE candidates observed as  $\gamma$ -ray/X-ray flares and those detected in the UV/O is not yet clear. We note that much smaller, stellar black holes, may also tidally disrupt stars. These would lead to  $\mu$ TDEs which might resemble ultra-long  $\gamma$ -ray bursts/X-ray flares and jetted-TDE candidates (Perets et al. 2016), but not the UV/O TDE-candidates on which we focus here.

Arcavi et al. (2014) classified the UV/O candidates into a sequence by their broad line spectral states: He-overbright cases; some with He II and H $\alpha$ ; and others with H $\alpha$  dominating. PS1-11af had broad absorption lines (beyond the scope of our emission modelling) but it is notable that the velocity widths were comparable to velocity widths of emission-line TDE candidates (Chornock et al. 2014). We note that Drake et al. (2011) classified another transient as an exotic supernova rather than a TDE, because the temperature was below predictions of early TDE theories. We disagree with this exclusion, since the properties were actually consistent with more recent UV/O TDE candidates, and suggest to include this as an additional TDE candidate (for our table of currently identified UV/O TDE-candidates, see the Appendix A). Our paper will study the spectroscopic features of TDE candidates, and analyse them using detailed photoionization models.

Previous studies by Gaskell & Rojas Lobos (2014) and Guillochon, Manukian & Ramirez-Ruiz (2014) tried to explain the spectral features of the UV/O TDE candidates. However, as we show in the following, none of the simple models suggested in the literature, typically involving AGN-like illumination, can actually explain the spectral properties of the candidates. In particular, though the line-ratios can be explained by models as suggested by Guillochon, Manukian & Ramirez-Ruiz (2014) and Gaskell & Rojas Lobos (2014), they fail to explain the *observed* equivalent width. We suggest a model which may overcome these difficulties, and provide novel predictions for the spectral temporal evolution. We consider how states similar to the observed line ratios and equivalent widths can arise in generic models of TDE, AGN outbursts, and other explosive events. Using models of photoionized spectra, we distinguish among luminous source spectra that can reproduce the observed lines.

Besides the failure of the simple picture to explain the observed spectral features, our current interpretation of candidate TDEs as bona-fide ‘real’ TDEs encounters several other difficulties. We complement our photoionization modeling with an analysis of these additional challenges and their implications, and briefly discuss other possible origins for the observed TDE candidates.

Our paper is organized as follows. We begin by describing our modeling of the spectral features of TDEs in Section 2, and show that none of the simple models can explain both the line ratios and equivalent widths seen in observations. We propose a novel model which could potentially resolve these difficulties (Section 2.2), and then discuss our results as well the possible origins of such nuclear flares (Section 3), and in particular possible alternatives to the TDE

origin, including subluminal AGN flaring and nuclear supernovae (Section 3.3.1).

## 2 MODELING

The principal luminous media in a TDE include the dense tidal stream of bound debris, which orbits round to shock its own tail and form an accretion disc; unbound debris escaping the system ballistically; and a radiation-driven wind. If the TDE continuum emission photoionizes circumnuclear gas clouds, like those of AGN, their line emissions may resemble an AGN’s broad emission line regions (BLRs) except evolving on shorter time-scales. In the following, we model the expected TDE spectral features, and compare them with the observed features. We find that current models are inconsistent with observed features, and we discuss a novel echo model that could be reconciled with observations.

### 2.1 Emission line ratios and equivalent widths

To interpret observations, we require predictions of both the He II(4686Å) and H $\alpha$ (6563Å) intensities, as well as the line ratios, the underlying continuum, and other lines that might appear. These synthetic observables are generic and time-independent: they should apply equally to slowly evolving structure under variable illumination (e.g. BLR during an AGN flare) or dynamically evolving clouds under a steady or variable radiation source (e.g. TDE debris). In order to do so, our calculations (below) follow photoionization models employing the CLOUDY code (Ferland et al. 2013). The standard approach (Baldwin et al. 1995; Korista & Goad 2004) is to compute emission line output of clouds across the ‘flux-density plane’, ( $n_{\text{H}}, \Phi_{\text{H}}$ ), where  $n_{\text{H}}$  is the cloud density, and  $\Phi_{\text{H}}$  is ionizing flux from a central isotropic source with a specified spectral energy distribution (SED), given by

$$\Phi_{\text{H}} = \frac{L}{4\pi r^2 \bar{\epsilon}}, \quad (1)$$

where  $\bar{\epsilon}$  is an effective mean ionizing photon energy for the given SED.

As calculated by Guillochon, Manukian & Ramirez-Ruiz (2014) and Gaskell & Rojas Lobos (2014), emission line ratios consistent with the He II-overbright state are attainable in specific cloud conditions, though they considered an AGN SED model of Mathews & Ferland 1987 (hereafter ‘MF1987’); moreover, see Strubbe & Murray 2015 for different conclusions). However, the observed ratios are a necessary but not *sufficient* constraint; any successful model should also provide the correct *equivalent widths* of the lines. As we show in the following, *all* the models, and in particular current SED models (constructed to be consistent with observations), on which we focus thus far fail to produce both the line ratios and the equivalent widths (but this is also true for the MF1987 model, considered here only for comparison with previous works).

If the line intensity emerging from a cloud is  $I_{\lambda}$  and the incident continuum is  $F_{\lambda}$ , the equivalent width (‘EW’) is  $W_{\lambda} \equiv I_{\lambda}/F_{\lambda}$ . The integrated EW of a composite system depends on the covering fraction of the clouds,  $\Omega$ . Observationally, emission lines with  $W_{\lambda} < 1\text{\AA}$  might be undetectable. Gezari et al. (2012), observing PS1-10jh, found an

<sup>1</sup> Realistically, TDE could just as well occur around active nuclei, but observers prefer to avoid false-positive identifications.

He II line luminosity of  $(9 \pm 1) \times 10^{40} \text{ erg s}^{-1}$ , which corresponds to  $W_{4686} = 66.4 \pm 13.9 \text{ \AA}$ ; while van Velzen et al. (2011) report a H $\alpha$  value  $W_{6563} = 87 \pm 5 \text{ \AA}$  for TDE2. The He II-overbright early state of ASASSN-15oi had an equivalent width  $W_{4686} = 99 \pm 13 \text{ \AA}$  (Holoien et al. 2016a). By visual inspection, other UV/O candidates' broad lines typically have equivalent widths of similar order (Wang et al. 2011; Drake et al. 2011; Holoien et al. 2014; Arcavi et al. 2014). These facts require models of the continuum and clouds that provide  $W_\lambda$  of at least a few  $\text{\AA}$ , for some covering factor. Therefore, models predicting smaller  $W_\lambda$  values are not viable matches for known UV/O transients, even if the line-ratios match.

Previous calculations (Gaskell & Rojas Lobos 2014; Guillochon, Manukian & Ramirez-Ruiz 2014) allowed a spatially extensive line-emitting medium, analogous to the BLR of an AGN, and employed the AGN-like MF1987 SED model. This SED model is inconsistent with observed AGN SEDs (Laor et al. 1997, and citations thereafter). Gaskell & Rojas Lobos (2014) and Guillochon, Manukian & Ramirez-Ruiz (2014) find that the He-overbright state (e.g. with the line ratio  $w \equiv I_{4686}/I_{6563} \approx 4$  observed in PS1-10jh) occurs naturally in specific photoionization conditions, without requiring helium-enriched gas. Guillochon, Manukian & Ramirez-Ruiz (2014) obtained time-dependent functions of  $(n_{\text{H}}, \Phi_{\text{H}})$  from hydrodynamic simulations of TDE streams, and showed that these tracks cross a He-overbright region of the flux-density plane (at least when the column  $N_{\text{H}} = 10^{23} \text{ cm}^{-2}$  exactly).

Roth et al. (2016) performed radiative transfer modelling of a TDE's central outflow, with a prescribed density profile, resulting in line emission (at an assumed velocity width) escaping from spherical layers near the continuum photosphere. He-overbright states with  $\text{EW} \gtrsim 100 \text{ \AA}$  (by inspection of their figures) appeared naturally in some configurations with outer radii  $\leq 2 \times 10^{15} \text{ cm}$ . (We might wonder whether such compactness would lead to significant intraday spectral variability.)

In our paper, we allow line-emission at larger spatial scales. In an approach that is initially similar to Gaskell & Rojas Lobos (2014), we focus on a variety of more modern SED models: an AGN spectrum with a spectral slope 1.2 (Baskin, Laor & Stern 2014); and another AGN case with 2.0 (these correspond to the *observed* range of slopes); a blackbody peaking at 4 Ryd; another at  $10^6 \text{ K}$ ; and a hotter  $10^7 \text{ K}$  blackbody (harder than the observed continuum). For comparison with the previous works we also run set of models using the MF1987 SED.

For each SED, we run several cubes of calculations: exploring a rectangle of  $(n_{\text{H}}, \Phi_{\text{H}})$  in steps of 0.1 dex, and saving depth profiles along the  $N_{\text{H}}$  or spatial axis. For greater resolution, and to check consistency, we rerun extra cubes where the maximum column was set to  $N_{\text{H}} = 10^{23}, 10^{24}, 10^{25} \text{ cm}^{-2}$ . We refer the interested reader to Appendix C for the technical details of the CLOUDY calculations.

Using these calculations, we densely map the range of possible values of H $\alpha$  to He II emission line ratio and He II equivalent widths obtainable when the luminous nuclear source is emitting steadily with a specified SED, and photoionizing a distant cloud (of solar composition). These computational surveys proceed in full generality, but we ap-

ply the results later (in post-processing) in the contexts of specific astronomical events. Table 1 presents the maximum attainable He II/H $\alpha$  line ratio ( $w_{\dagger}$ ) for each SED model, the cloud parameters where this occurs, and the equivalent widths of five emission lines in these conditions (assuming some covering factor,  $\Omega$ ). Fig. 1 shows the distribution of CLOUDY results in the region of parameter-space near the peak. A dot is plotted for every result pair  $(I_{4686}/I_{6563}, W_{4686})$  obtained from each input condition  $(N_{\text{H}}, n_{\text{H}}, \Phi_{\text{H}})$  in the photoionization parameter cube. Qualitatively similar plots can be generated in absolute terms of He II line luminosity  $(I_{4686}/I_{6563}, L_{4686})$ . For a specific application, the observation of PS1-10jh is plotted in cyan, where, using the results and plots of Gezari et al. (2015), the He II line luminosity is  $L_{4686} = (9 \pm 1) \times 10^{40} \text{ erg s}^{-1}$ ; the blackbody flux of the observed continuum under the line was  $F_{\text{o}} \approx (1.7 \pm 0.3) \times 10^{-17} \text{ erg cm}^{-2} \text{ s}^{-1} \text{ \AA}^{-1}$ . The fitted temperature ( $T_{\text{o}} \approx 3 \times 10^4 \text{ K}$ ) implies a photospheric luminosity  $L_{\text{o}} \approx 8.7 \times 10^{43} \text{ erg s}^{-1}$ . The He II line's equivalent width is  $W_{4686} = 66.4 \pm 13.9 \text{ \AA}$ .

For the sake of illustration, we assume a covering factor  $\Omega = 0.1$ , but the results for any chosen  $\Omega$  can be easily obtained by moving the points appropriately (e.g left, if  $\Omega$  is reduced). The set of solutions that would be consistent with observations for smaller covering factors ( $\Omega < 0.1$  a free parameter) are plotted in black. AGN-like spectra (top row of the Figure) produce line ratios compatible with PS1-10jh under a wide range of conditions, however, the He II equivalent widths are *inconsistent* with *any* AGN-like models, even for covering factor much larger than would be realistically expected (the MF1987 case could work only in unrealistic extreme cases, requiring huge covering factors,  $\Omega \gtrsim 0.82$ , and positions closer than 3 light days from the nucleus).

Given the failure of these models, we now consider other types of source models, in order to try to overcome the EW problem. In particular, we consider a set of simple blackbody SED models. For the 4Ryd,  $10^6 \text{ K}$  and  $10^7 \text{ K}$  blackbody models (bottom row of the Figure) there is an extensive range of plausible solutions that satisfy observational constraints on *both* the line ratio and EW, either for the standard covering factor and even for smaller values ( $\Omega \leq 0.1$ ). The potential disadvantage of these hot sources is that they would be difficult to reconcile with the observed  $T_{\text{o}} \approx 3 \times 10^4 \text{ K}$  continuum. Nevertheless, in the following, we suggest a generic scenario which can accommodate these constraints when the central luminous source is non-stationary and a light echo occurs.

## 2.2 A novel scenario: Light-echo photoionization of nuclear clouds

A hard ionizing continuum that peaks at  $h\nu \sim 4 \text{ Ryd}$  and a high density gas  $n_{\text{H}} \sim 10^{12} \text{ cm}^{-3}$  is required to produce both a strong He II  $\lambda 4686$  emission-line and a large He II/H $\alpha$  line ratio. The hard continuum induces high gas temperatures, which makes the He $^{++}$  recombination coefficient larger relative to H $^{+}$ ; and the high gas density makes the gas optically thick to H $\alpha$  (see Strubbe & Murray 2015). However, observations in the optical of He II-bright TDE candidates are consistent with a black-body continuum source with a temperature  $T_{\text{BB}}$  of a few  $10^4 \text{ K}$  only (e.g. Gezari et al. 2012). Two scenarios can alleviate this discrepancy. In the first scenario, two continuum sources exist concurrently: a 'cold'

**Table 1.** CLOUDY model conditions for a given source SED that give the peak ratio of He II(4686Å) to Hα(6563Å) emission line intensities ( $w_{\dagger} \equiv I_{4686}/I_{6563}$ ). At the peak, the hydrogen column density, number density, and ionising flux are labelled ( $N_{\dagger}, n_{\dagger}, \Phi_{\dagger}$ ). The last five columns give the equivalent widths of emission lines, calculated for full coverage ( $\Omega=1$ ) ( $W_{\lambda}$ ) for He II, Hα, Hγ, C IV, and Mg II emission lines. By rows, the illuminating SED was Mathews & Ferland (1987); AGN with slope 1.2; AGN with slope 2.0; 4Ryd blackbody;  $10^6$ K blackbody;  $10^7$ K blackbody.

SED	$\log \bar{\epsilon}$	$\log N_{\dagger}$	$\log n_{\dagger}$	$\log \Phi_{\dagger}$	$w_{\dagger}$	$\log W_{4686}$	$\log W_{6563}$	$\log W_{4340}$	$\log W_{1549}$	$\log W_{2798}$
	(eV)	( $\text{cm}^{-2}$ )	( $\text{cm}^{-3}$ )	( $\text{cm}^{-2} \text{s}^{-1}$ )		(Å)	(Å)	(Å)	(Å)	(Å)
MF1987	1.881	23.9	11.6	22.7	6.92	1.32	0.624	0.155	1.84	0.0182
AGN1.2	2.118	23.8	11.6	22.4	5.15	1.11	0.600	0.00589	1.76	-0.139
AGN2.0	2.065	23.7	11.2	22.3	4.52	0.765	0.312	-0.164	1.43	-0.364
4Ryd	1.572	23.8	12.2	23.0	7.49	2.94	2.63	1.75	1.80	1.27
$10^6$ K	2.369	23.2	13.1	25.3	7.66	2.73	2.43	1.59	—	—
$10^7$ K	3.367	22.8	13.7	24.7	6.42	5.29	5.07	4.04	-1.33	—

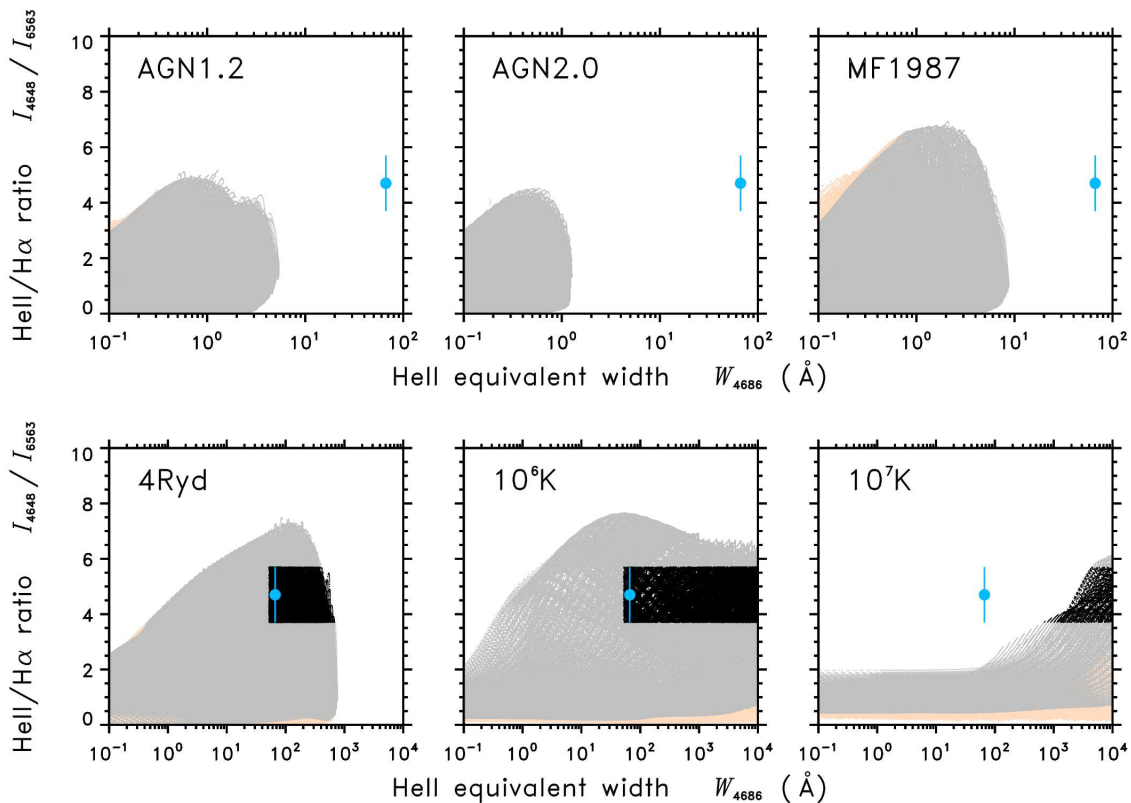


**Figure 1.** The distribution of possibilities for the  $I_{4686}/I_{6563}$  line ratio vs He II equivalent width, assuming a nominal covering factor  $\Omega = 0.1$ . The top panels assume an AGN-like central source; the bottom panels assume a steady blackbody source. The cyan datum shows the observed line ratio and He II equivalent width for PS1-10jh. Black areas are compatible with observations, for the fiducial  $\Omega$  or smaller. Grey areas fail to match. Orange areas are physically rejected since they would reside inside the photosphere. The central source luminosity is assumed to be time-independent, and was normalized to match the observed continuum around wavelength 4686Å. Note that a smaller choice of  $\Omega$  corresponds to a proportional translation of dots leftwards parallel to the horizontal axis. Consistent models in this context would require  $\Omega > 9.7 \times 10^{-3}$  for the 4Ryd model;  $\Omega > 2.3 \times 10^{-5}$  for  $10^6$ K; and  $\Omega > 1.1 \times 10^{-7}$  for  $10^7$ K models.

source which is observed in the optical; and another ‘hot’ source (e.g. a black body with  $kT_{\text{BB}} \sim 4$  Ryd) which ionizes the line-emitting gas. As the ‘hot’ source cools, the ionizing continuum becomes softer, and the object transforms from a He II- to H $\alpha$ -bright. In the second scenario, there is a single continuum source only. The source cools from a very high  $T$  (e.g.  $T_{\text{BB}} \sim 10^9$  K) to the observed  $T_{\text{BB}} \sim 10^4$  K. The line-emitting gas is located at a distance of the order of several to a few tens of light-days from the continuum source and from our line-of-sight to the source. The observed line emission is delayed w.r.t. the observed continuum emission. Thus, in He II-bright objects, we measure line emission which corresponds to a continuum source with  $kT_{\text{BB}} \sim 4$  Ryd (or more), when the observed continuum source itself has already cooled to  $T_{\text{BB}} \sim 10^4$  K. The object transforms from He II- to H $\alpha$ -bright when the delayed line emission corresponds to an ionizing continuum with  $T_{\text{BB}} \lesssim 10^5$  K. The second scenario has a few consequential implications, which are described below. We do not include in our model the relatively constant X-ray source that is observed in some TDE candidates (Holoien et al. 2016a,b), as its contribution to the flux of ionizing photons is negligible. The X-ray emission may be produced by coronal-type emission or by shocked ISM gas (first or second scenario, respectively).

### 2.2.1 Model calculations

The continuum during the broad line phases of the UV/O candidates indicates temperatures of  $10^4$  K  $\lesssim T \lesssim 10^5$  K. In time-independent modeling, a luminous source at such temperatures seems unable to photoionize clouds to produce He II and H $\alpha$  equivalent widths in the observed range. Hotter sources could induce emission lines with the observed equivalent widths, but require covering factors orders of magnitude smaller. The lax constraints on  $\Omega$  are favourable, but the high-temperature continuum is inconsistent with observation. This leads us to the possibility of a time-dependent source, which might provide the best features of both the low- and high-temperature SEDs.

Firstly suppose that the central source was a sudden energetic detonation in a (possibly inhomogenous) gaseous medium, at a super-Eddington rate. It might have been a tidal disruption event, a large-amplitude AGN flare, a peculiar kind of superluminous supernova, or any unrecognised new class of explosion with sufficient energy and brevity. Regardless of what the specific injection mechanism might have been, the central medium will expand as an opaque, radiation-dominated wind or blast-wave. If the injection was abrupt, then the photosphere expands adiabatically with a temperature vs radius relation of  $T \propto 1/R$ . If there was continuous energy injection, due to the power of a hidden, central accreting source, then different relations govern the observable light curve.

Next, in order to set spatial and temporal scales, suppose that the hot initial ‘flash’ phase lasted less than a few days. The opaque photosphere, dominated internally by radiation pressure, expands and cools. As the initial flash of hard radiation propagates outwards, it photoionizes circumnuclear clouds or dense debris (perhaps within several light-days of the center). Depending on distance and the evolving luminosity, some clouds emit lines in a He-over-bright state, including the strong-EW mode in our  $10^7$  K calcu-

lations. Light from the photosphere reaches telescopes at Earth directly, but line emission from the clouds is delayed by the light-travel time to the cloud ( $R_c/c$ ). Thus the He-overbright clouds’ emission is superimposed as a light-echo on a later, expanded and cooled view of the nucleus photosphere. Obtaining the observed equivalent widths ( $W \sim 60\text{\AA}$ ) and underlying continuum temperature ( $10^4$  K to  $10^5$  K) implies constraints on the photospheric temperature and luminosity evolution, the covering factor and location of the cloud. From the column density ( $N_{\text{H}}$ ) assumed in each candidate photoionization model, the total mass of clouds is derivable.

In the light-echo model, we suppose that the source is an optically thick photosphere of the flare or wind expanding according to power-laws in time:

$$T \propto t^a \quad (2)$$

$$L \propto t^b \propto T^{b/a} . \quad (3)$$

For a blackbody emitting photosphere, the radius

$$R \propto T^x \quad (4)$$

has index  $x = [(b/a) - 4]/2$ . For an explosion expanding adiabatically at constant velocity,  $a = -1$  and  $b = -2$ . For a relativistic event driven by a central power source ( $P \propto t^q$ ), we might have  $a = (q - 2)/4(q + 2)$ ,  $b = (2 + 3q)/(2 + q)$  (Blandford & McKee 1976; Cohen & Piran 1999). For some models of the rising phase of a TDE, the indices  $a = -7/36$ ,  $b = 11/9$  (Strubbe & Quataert 2009; Lodato, King & Pringle 2009). For illustrations in this paper, we assume the simple adiabatic model.

We explore a broad realm of possibilities across the ( $N_{\text{H}}, n_{\text{H}}, \Phi_{\text{H}}$ ) space, while correcting the model continuum for the time-lagged expansion of the photosphere. Fig. 2 (top row) shows the He II line luminosities and He II/H $\alpha$  ratio, in the context of PS1-10jh and its parameters, and assuming a constant-velocity adiabatic expansion of the central source. Bottom panels of Fig. 1 are corresponding plots where the horizontal axis is the He II equivalent width. Black dots are compatible with observations, for our fiducial covering factor or a smaller value ( $\Omega \leq 0.1$ ). In addition to rejecting models where the cloud would reside underneath the photosphere, we also omit cases where  $R_c$  would exceed 60 light days, as this would be beyond the characteristic scale implied by the 22 day rise time of the observed light-curve. The light-echo model reduces the equivalent widths for the hotter blackbody SED scenarios. When the covering factor is a free parameter, there are still many acceptable fits that have small  $\Omega$ . The limits from PS1-10jh would require  $\Omega > 0.027$  for the 4Ryd model;  $\Omega > 7.6 \times 10^{-4}$  for  $10^6$  K; and  $\Omega > 8.6 \times 10^5$  for  $10^7$  K.

The emission line broadening results from gas motions which are transverse to the impinging ionizing radiation. Strubbe & Murray (2015) pointed out that a velocity gradient which is parallel to the radiation reduces the gas opacity. This increases H $\alpha$  emission, and thus reduces the He II/H $\alpha$  line ratio. We carried out photoionization calculations with ‘turbulent’ velocity which corresponds to the observed line width in PS1-10jh ( $\sigma_{\text{turb}} = 5400$  km s $^{-1}$ ). These calculations indeed result in He II/H $\alpha < 1$ .

Fig. 3 shows the predicted values of C IV and Mg II emission line luminosities, in comparison to the He II luminosity (in the echo model assuming  $\Omega = 0.1$ ). The selection of credible solutions for PS1–10jh (marked black) relies only on the H $\alpha$  and He II emission properties, as in Fig. 2. Among the set of solutions that are compatible with PS1–10jh, the C IV and Mg II luminosities and equivalent widths can in some cases be comparable to the He II value, or it can be less, but we do not find any cases where they would be more than a few times stronger than the He II.

Fig. 4 plots the distribution of cloud mass and position ( $M_c, R_c$ ) for these realistic possibilities, in our blackbody light-echo results. Each dot corresponds to one of the successful solutions that were marked black in Fig. 2. Now the colour scale indicates  $\Omega$  (as a fitted parameter). The likely locations are at light-days or tens of light-days from the central source, which agrees with the light-echo expectations. In all cases investigated, we find the following:

- The median cloud masses are subsolar. Taken without bias across the whole parameter space, the masses tend to be planetary in scale. Masses on the order of  $\sim 0.1 m_\odot$  are possible, but require fine-tuning.

- Cloud positions at  $\sim 10$  light days occur naturally, without premeditation or fine-tuning. The implied covering factors are mostly moderate ( $10^{-3} \leq \Omega \leq 10^{-1}$ ), which retrospectively justifies our fiducial assumptions, and supports the light echo scenario.

- At the favoured cloud locations of  $\sim 10$  light days, the orbital velocities would be low enough to solve the velocity problem of the UV/O optical candidates (e.g. discussed by [Arcavi et al. 2014](#)). The emission line widths are unrelated to the inner nucleus where the tidal disruption or luminous flare occurs (see Appendix B). They may simply characterize the motions of pre-existing clouds in the impoverished BLR of a previously dormant, declining or erratic weak AGN.

Interestingly, several recent papers have reported infrared light-echo effects from dusty media around TDE candidates. [Jiang et al. \(2016\)](#) and [van Velzen et al. \(2016b\)](#) infer clouds at tens of light days from the nucleus, which is consistent with the cloud locations in our photoionization models. [Dou et al. \(2016\)](#) find IR light echo effects over longer time-scales, implying more clouds a few light years farther out.

### 3 DISCUSSION

As we discussed above, any acceptable type of model for UV/O TDE-candidates should be able to accommodate both the observed line ratio *and* the EW constraints, while *none* of the previously suggested, steadily illuminated models stands to the test. Independent of the origin of the TDE candidates, our echo scenario could reproduce the observations, for various assumed types of transients. Nevertheless, it can constrain details of the explosive origin. In the following subsections, we first discuss the implications of the light-echo model, then overview some of the difficulties with the TDE scenario for the observed UV/O candidates. We consider possible alternatives to TDE origins, including nuclear SNe (in the light-echo model), or intermittency in sub-luminous/starved AGNs.

### 3.1 Implications of the light-echo model

#### 3.1.1 Implications for the continuum source

Assuming a single continuum source that cools from  $T_{\text{BB}} \sim 10^9$  to  $10^4$  K enables evaluation of several key properties. Our goal here is to provide qualitative order-of-magnitude estimates, rather than quantitative calculations, since the latter require extensive numerical modeling which is beyond the scope of this paper. We make two additional simplifying assumptions. First, the continuum source is a spherical black body, which cools through adiabatic radial expansion with an adiabatic index of  $\gamma = 4/3$  (i.e. dominated by radiation pressure). Second, all relevant time scales are of the order of the light travel time from the continuum source to the line emitting gas, i.e.  $\tau \sim R_c/c$ , where  $R_c$  is the distance between the source and the gas, and  $c$  is the speed of light. The first approximation is a rough one, as gas with  $T \leq 10^6$  K can cool through line emission, which breaks the adiabatic approximation and slows the expansion.

The flux of H-ionizing photons ( $h\nu \geq 1$  Ryd) that is emitted by a black-body with a temperature  $T_{\text{BB}}$  can be approximated by

$$\Phi \simeq \frac{4\pi k^3 T_{\text{BB}}^3}{h^3 c^2} \zeta(3) = 1.5 \times 10^{29} T_{\text{BB},6}^3 \text{ cm}^{-2} \text{ s}^{-1}, \quad (5)$$

where  $k$  is the Boltzmann constant,  $h$  is Planck's constant,  $\zeta$  is the Riemann zeta function [ $\zeta(3) \simeq 1.2$ ] and  $T_{\text{BB}} = 10^6 T_6$  K.<sup>2</sup> The expression is correct within 2% and 30% for  $T_6 \geq 0.5$  and 0.1, respectively. There are an optimal  $T_{\text{BB}}$  ( $T_{\text{opt}}$ ) and a corresponding optimal  $\Phi$  at the illuminated face of the gas ( $\Phi_{\text{opt}}$ ) which produce maximal He II and minimal H $\alpha$  emission. These two parameters are somewhat degenerate and depend on the gas column. They can be roughly approximated by  $T_{\text{opt}} \sim 10^6$  K and  $\Phi_{\text{opt}} \sim 10^{23} \text{ cm}^{-2} \text{ s}^{-1}$ . The radius of a black body with  $T = T_{\text{opt}}$  that produces  $\Phi_{\text{opt}}$  at  $r = R_c$  is

$$R_{\text{opt}} \approx \sqrt{\frac{\Phi_{\text{opt}}}{\Phi}} R_c = 2.1 \times 10^{13} T_{\text{opt},6}^{-1.5} \Phi_{23}^{0.5} r_{10\text{ld}} \text{ cm}, \quad (6)$$

where  $\Phi_{\text{opt}} = 10^{23} \Phi_{23} \text{ cm}^{-2} \text{ s}^{-1}$  and  $R_c = 10 r_{10\text{ld}} \text{ ld} = 2.6 \times 10^{16} r_{10\text{ld}} \text{ cm}$ , which corresponds to the observable time-scale of spectral variations ([Gezari et al. 2012](#); [Holoien et al. 2016b](#)). The assumption of adiabatic expansion yields an initial radius of continuum source of

$$R_i = \left( \frac{T_{\text{opt}}}{T_i} \right)^{\frac{1}{3(\gamma-1)}} R_{\text{opt}} = 2.1 \times 10^{10} T_{\text{opt},6}^{-0.5} T_{i,9}^{-1} \Phi_{23}^{0.5} r_{10\text{ld}} \text{ cm}, \quad (7)$$

where  $T_i = 10^9 T_{i,9}$  K is the initial  $T_{\text{BB}}$  of the source. Mutatis mutandis, the final radius of the source is

$$R_f \sim 2.1 \times 10^{14} T_{\text{opt},6}^{-0.5} T_{f,5}^{-1} \Phi_{23}^{0.5} r_{10\text{ld}} \text{ cm}, \quad (8)$$

where  $T_f = 10^5 T_{f,5}$  K. We use  $T_f \sim 10^5$  K as the final  $T_{\text{BB}}$ , rather than  $10^4$  K, since at  $T \sim 10^5$  K the source likely no longer expands significantly, and most of the cooling is attributed to radiative losses (see above).

<sup>2</sup> Although the discussion focuses on line emission of He II which requires photons with  $h\nu \geq 4$  Ryd, we include photons already from  $h\nu \geq 1$  Ryd in  $\Phi$ , as this is the standard definition of  $\Phi$  in photoionization codes (e.g. CLOUDY).

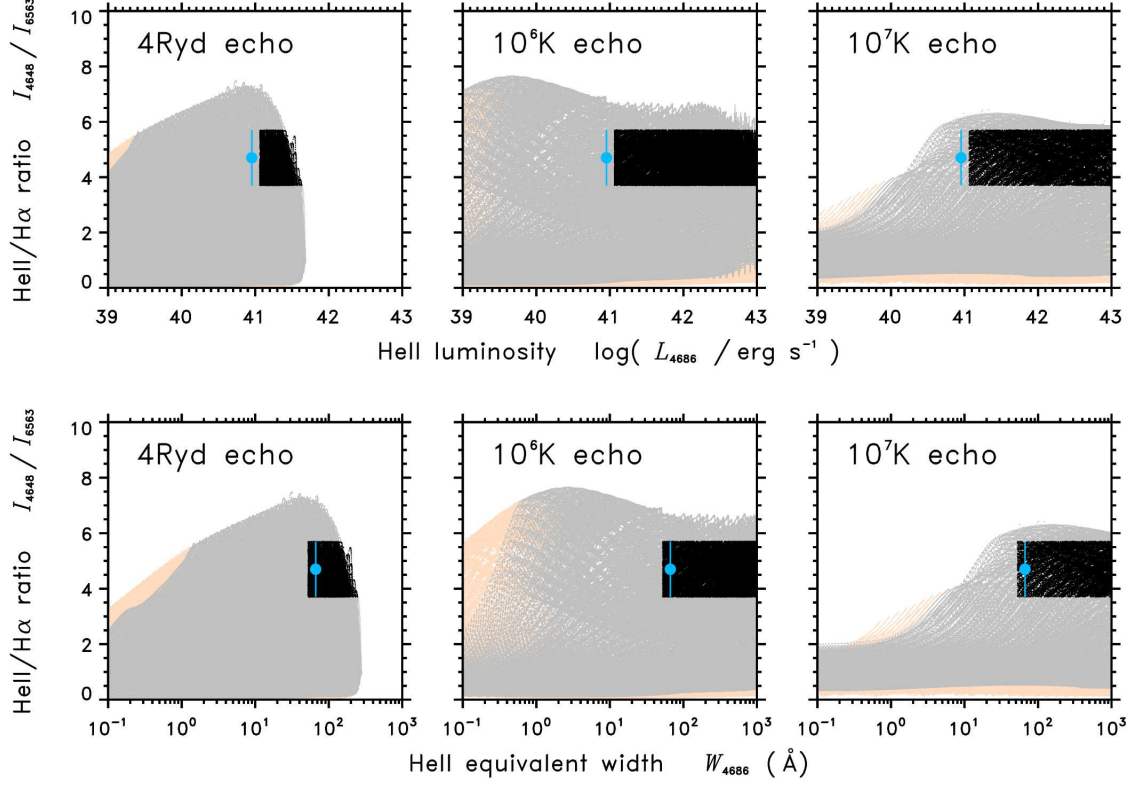


**Figure 2.** The distribution of line ratios vs He II line luminosity (top row) and He II equivalent widths (bottom row) in blackbody light-echo models. The assumed photosphere expands adiabatically at constant velocity, illuminating a cloud with covering factor  $\Omega = 0.1$ . As in Fig. 1, black dots are solutions consistent with observations (when  $\Omega \leq 0.1$ ); the PS1–10jh data are the cyan dot; unphysical solutions are orange; observationally incompatible points are grey. Note that a smaller choice of  $\Omega$  corresponds to a proportional translation of dots leftwards parallel to the horizontal axis.

The expansion velocity of the continuum source can be approximated by

$$v_{\text{exp}} \sim \frac{R_f}{R_c/c} = 2400 T_{\text{opt},6}^{-0.5} T_{f,5}^{-1} \Phi_{23}^{0.5} \text{ km s}^{-1}. \quad (9)$$

Note that  $v_{\text{exp}}$  is independent of the assumed  $R_c$ . The He II-bright state is produced from  $T_{\text{BB}} = 10^6 \text{ K}$  down to  $10^5 \text{ K}$ , i.e. 1 dex in  $T_{\text{BB}}$ . Since  $T_{\text{BB}} \propto R^{-1}$  (eq. 7), an object will be in a He II-bright state for a period of

$$\Delta t \approx 10 R_{\text{opt}} / v_{\text{exp}} = 10 T_{\text{opt},6}^{-1} T_{f,5} r_{10\text{ld}} \text{ d}, \quad (10)$$

where we used eq. (6). Assuming isentropic expansion and using eq. (9) we can evaluate the total mass  $M$  of the continuum source. The velocity of isentropic expansion is approximately

$$v_{\text{ise}} \approx \frac{2}{\gamma - 1} \sqrt{\gamma \frac{a T_i^4 / 3}{M (4\pi R_i^3 / 3)^{-1}}}, \quad (11)$$

where  $a = 4\sigma/c$ , and  $\sigma$  is the Stefan-Boltzmann constant (e.g. Zel'dovich & Raizer 1967). Taking  $v_{\text{ise}} = v_{\text{exp}}$  and inserting eq. (7) yields  $M \approx 4 \times 10^4 T_{i,9} T_{\text{opt},6}^{-0.5} T_{5,f}^2 \Phi_{23}^{0.5} r_{10\text{ld}}^3 m_{\odot}$ , which is an unreasonable value for an explosion of stellar progenitor. We note that slightly reducing the assumed  $\gamma$  to  $\gamma = 5/4$  yields  $M \sim 10 m_{\odot}$  (and a corresponding  $R_i \sim 10^9 \text{ cm}$ ). The smaller value of  $\gamma$  is relevant only for the highest  $T$  and small  $R$ , where the conditions in the source may be favourable for pair production, reducing  $\gamma$

below  $\gamma = 4/3$ . (Plausibly, some entrainment of upswept circumnuclear gas might also alter  $\gamma$ .) The total bolometric luminosity as a function of  $T$  of the continuum source is

$$\begin{aligned} L_{\text{bol}} &= 4\pi R^2 \sigma T_{\text{BB}}^4 = 4\pi R_{\text{opt}}^2 \sigma T_{\text{opt}}^2 T_{\text{BB}}^2 \\ &= 3.2 \times 10^{45} T_5^2 T_{\text{opt},6}^{-1} \Phi_{23}^2 r_{10\text{ld}}^2 \text{ erg s}^{-1}, \end{aligned} \quad (12)$$

where  $T_{\text{BB}} = 10^5 T_5 \text{ K}$ . This estimated  $L_{\text{bol}}$  is broadly consistent with observations (van Velzen et al. 2011; Cenko et al. 2012a; Chornock et al. 2014; Cenko et al. 2016; Holoien et al. 2016b). Thus, an adiabatic expansion predicts that for  $v_{\text{exp}} t \gg R_{\text{in}}$ ,  $L_{\text{bol}} \propto t^{-2}$ . The total energy that is emitted during the adiabatic-expansion phase is

$$\begin{aligned} E &\sim \int_0^{R_c/c} L_{\text{bol}} dt \simeq \frac{4\pi \sigma R_{\text{opt}}^4 T_{\text{opt}}^4 R_c}{R_i R_f c} \\ &= 3 \times 10^{55} T_{\text{opt},6}^{-1} T_{i,9} T_{f,5} \Phi_{23}^3 r_{10\text{ld}}^3 \text{ erg}, \end{aligned} \quad (13)$$

which is larger by a factor of  $\sim 10^3$  compared to observed energies of super-luminous SNe (Gal-Yam 2012; Inserra et al. 2013; Vreeswijk et al. 2014; Dong et al. 2016). The tension between the energy implied by eq. (13) and the observed one may be reduced by noting that observations are carried out in the optical, where a source with  $T_{\text{BB}} \gtrsim 10^5 \text{ K}$  has negligible emission. Replacing  $R_i$  with  $R_{\text{opt}}$  in eq. (13) (i.e., starting the integration at  $T_{\text{BB}} = 10^6$  rather than  $10^9 \text{ K}$ ) yields  $E \sim 3 \times 10^{52} \text{ erg}$ , consistent with observations. Detailed tests show that the energy and mass within the photosphere are sensitive to details of different  $\gamma$  and models of

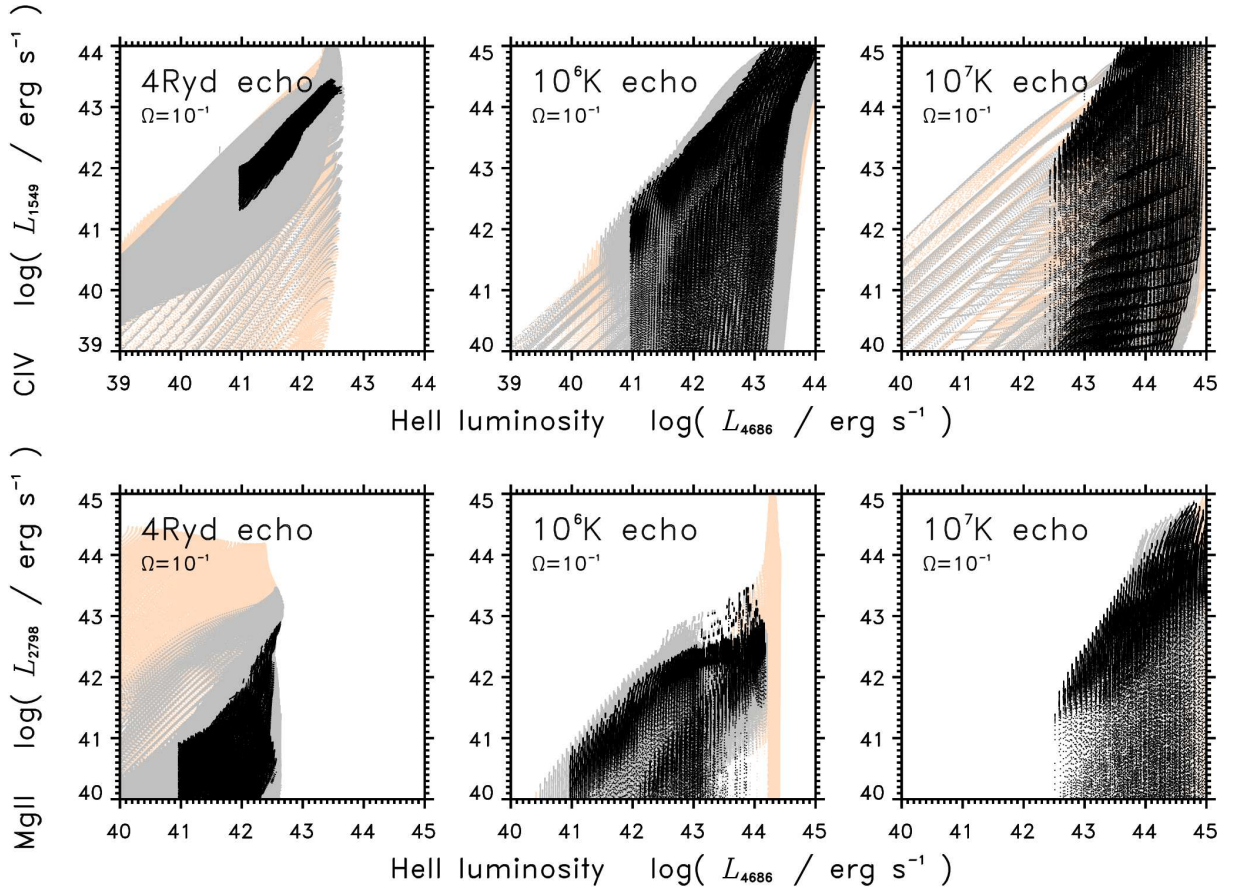


**Figure 3.** The distribution of predictions for luminosities of CIV and MgII emission lines (vertical axes) from black-body light-echo models. Solutions have been selected and colored (as in Fig.1) for their consistency with H $\alpha$  and HeII observations of PS1–10jh. The shown CIV and MgII properties are unforced, independent predictions. Horizontal axes show the HeII luminosities.

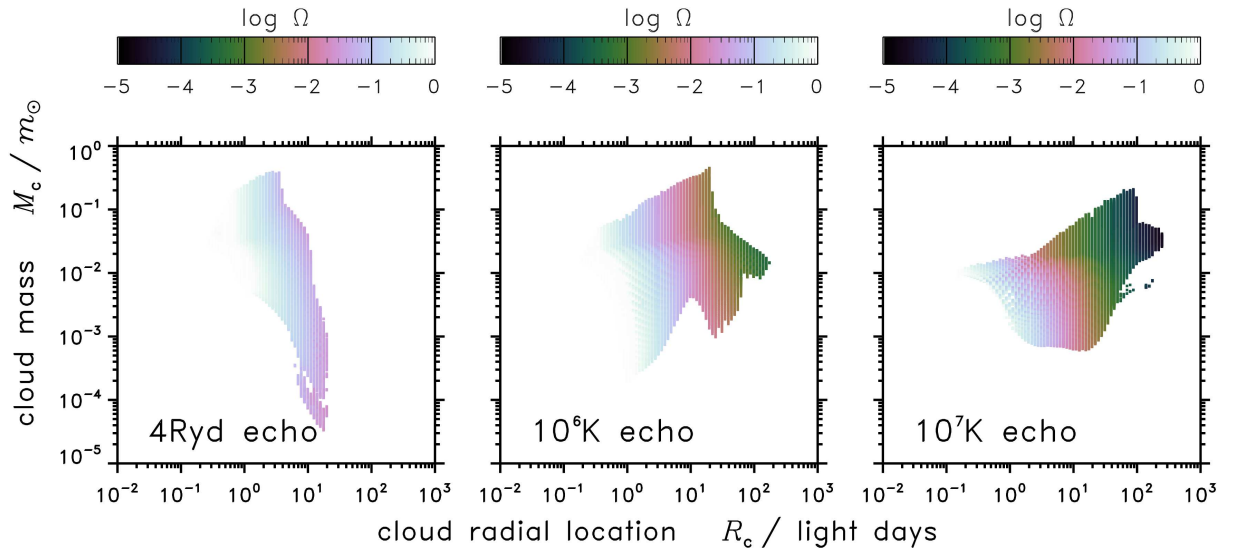


**Figure 4.** The distribution of possible cloud masses ( $M_c$ ) and locations ( $R_c$ ) that are compatible with PS1–10jh observations, for some covering factor ( $\Omega$ , now a fitted parameter). Panels show three blackbody light-echo models, as annotated. Colours indicate the cloud covering factor. Only the observationally consistent solutions (black in Fig. 1) are shown. The implied cloud mass never exceeds a subsolar value, and is extremely subsolar in most solutions.



the photosphere's expansion. The properties of the external photoionized cloud are more robustly constrained.

### 3.1.2 Implications for the line-emitting gas

To produce a He II-bright state, the line-emitting gas must react to variations in the ionizing continuum quicker than the variability time-scale of the continuum source. Two time-scales affect the gas: the ionization and recombination time-scales. The gas reacts to changes in the continuum on the longer of these two time-scales. We continue to use  $\tau_{\text{var}} \equiv R_c/c = 8.6 \times 10^5 r_{10\text{ld}} \text{ s}$  as the variability time-scale of the continuum source. The ionization time-scale  $\tau_{\text{ion}}$  can be estimated as follows. The photoionization cross-section of  $\text{He}^+$  that is averaged over a black-body continuum ( $\bar{\sigma}$ ) can be approximated by

$$\bar{\sigma} \approx \begin{cases} 1.41 \times 10^{-18} T_6 \text{ cm}^2, & \text{for } 0.1 \leq T_6 < 0.3 \\ 1.10 \times 10^{-19} T_6^{-1.7} \text{ cm}^2, & \text{for } T_6 \geq 0.3 \end{cases}, \quad (14)$$

where we use the expression for  $\sigma(\nu)$  from [Verner & Ferland \(1996\)](#). The approximation is correct within a factor of 3. The implied  $\tau_{\text{ion}} \equiv 1/\bar{\sigma}\Phi$  is

$$\tau_{\text{ion}} \approx \begin{cases} 7 \times 10^{-6} \Phi_{23}^{-1} T_6^{-1} \text{ s}, & \text{for } 0.1 \leq T_6 < 0.3 \\ 9 \times 10^{-5} \Phi_{23}^{-1} T_6^{-1.7} \text{ s}, & \text{for } T_6 \geq 0.3 \end{cases}. \quad (15)$$

Thus,  $\tau_{\text{ion}} \ll 1 \text{ s}$  for  $\Phi_{23} \sim 1$  and  $T_{\text{opt},6} \sim 1$ , and is negligible compared to  $\tau_{\text{var}}$ . The assumption of adiabatic expansion yields  $\tau_{\text{ion}} \ll \tau_{\text{var}}$  also for  $T_6 \sim 1000$ , i.e. when the continuum source is at maximum  $T_{\text{BB}}$ , since  $\Phi_2 = \Phi_1 T_2/T_1$  (eqs. 5 and 7). The constraint on the recombination time scale,  $\tau_{\text{rec}} \equiv 1/\alpha n_{\text{gas}} < \tau_{\text{var}}$ , implies a lower limit on the gas number density  $n_{\text{gas}}$ , where  $\alpha$  is the recombination coefficient. We approximate the dependence of  $\alpha$  of  $\text{He}^{++}$  on  $T_{\text{gas}}$  by  $\alpha \approx 10^{-7} T_{\text{gas}}^{-1.07} \text{ cm}^3 \text{ s}^{-1}$  ([Verner & Ferland 1996](#)), which is accurate within a factor of 2.5 in the  $10^4 \leq T_{\text{gas}} \leq 10^9 \text{ K}$  range. The implied constraint on the gas density is

$$n_{\text{gas}} > \frac{1}{\alpha} \frac{1}{R_c/c} \approx 3 \times 10^6 T_{\text{gas},5}^{1.07} r_{10\text{ld}}^{-1} \text{ cm}^{-3}, \quad (16)$$

where  $T_{\text{gas}} = 10^5 T_{\text{gas},5} \text{ K}$ .<sup>3</sup> This value of  $n_{\text{gas}}$  is well below  $n_{\text{gas}} \sim 10^{12} \text{ cm}^{-3}$  which is required by photoionization calculations to produce the observed high He II/H $\alpha$  line ratio.

## 3.2 Puzzles and difficulties for the TDE model

Several puzzles and problems emerge from observational studies of TDE candidates (see [Komossa 2015](#)), and may suggest that these events might not arise from tidal disruptions by MBHs, but rather from other sources. Here we only focus on issues relating to our results, and later discuss possible alternative origins.

1. In some systems, the inferred mass accretion is subsolar (see also discussion in section 2.2.1), and indeed much less than any likely donor star. For UV/O candidates, the most credible estimates appear subsolar ([Renzini et al. 1995](#); [Gezari et al. 2012](#); [Chornock et al.](#)

[2014](#); [Holoien et al. 2014](#)). ASASSN-14ae was discovered after its peak, but the accretion was only  $\gtrsim 0.001 m_{\odot}$  ([Holoien et al. 2014](#)). More clearly subsolar events include PS1-11af with  $0.002 m_{\odot}$  ([Chornock et al. 2014](#)); ASASSN-14li with  $0.004 m_{\odot}$  ([Holoien et al. 2016a](#)); ASASSN-15oi with  $0.003 m_{\odot}$  ([Holoien et al. 2016a](#)); PS1-10jh with  $0.012 m_{\odot}$  ([Gezari et al. 2012](#)); and  $0.004 m_{\odot}$ ,  $0.11 m_{\odot}$  for two transients of [Gezari et al. \(2008\)](#). It was suggested that these were partial disruption events. On the other hand, [Guillochon, Manukian & Ramirez-Ruiz \(2014\)](#) fitted PS1-10jh light-curves to simulations of a  $4 m_{\odot}$  star in a sub-Eddington TDE without a strong wind. Our light-echo model of the He II-overbright spectral line state also indicates subsolar masses for the clouds. It might be that the accretion process was radiatively inefficient for some unknown reason; perhaps because the tidal stream's self-intersection shock has been delayed by orbital precession effects or other complications ([Guillochon & Ramirez-Ruiz 2015](#); [Piran et al. 2015](#); [Svirski, Piran & Krolik 2015](#)). If not, the low mass indicators reveal something unexpected about the accretion source.

If a normal star was only partially disrupted (e.g. [Guillochon & Ramirez-Ruiz 2013](#)) this would explain the low mass budget of the luminous transient, but flaring should eventually recur on timescales comparable to the orbital period of the remnant stellar core. Since no secondary flare has been reported, the partial TDE scenario would require orbital periods longer than several years (in every TDE candidate).

2. For the UV/O TDE candidates, the emission line widths tend to be less than the orbital velocities expected at  $R_t$ , or else the emission region is radially much larger than expected from stellar disruption ([Gezari et al. 2009, 2012](#); [Arcavi et al. 2014](#); [Chornock et al. 2014](#)). A potential solution could invoke debris circularization occurring far from the tidal-disruption radius, ([Piran et al. 2015](#); [Svirski, Piran & Krolik 2015](#)) but whether this is indeed the culprit is still an open question. We further discuss this issue and present the relevant data in the Appendix B.

3. Reviewing a set of UV/O candidates, [Arcavi et al. \(2014\)](#) noted that most TDE host galaxies seem weak in star formation, and several belong to the rare E+A 'post-starburst' type. Exceptionally, [Holoien et al. \(2014\)](#) report a candidate in a spiral galaxy. E+A 'post-starburst' galaxies show stellar absorption lines indicating a stellar population truncated at a few Gyr age, and ongoing star formation is weak or regionally limited ([Dressler & Gunn 1983](#); [Yamauchi & Goto 2005](#); [Brown et al. 2009](#); [Pracy et al. 2014](#)). They often exhibit disturbed morphologies or close tidally interacting companion galaxies ([Yang et al. 2004](#); [Kewley, Geller & Barton 2006](#); [Goto et al. 2008](#); [Pracy et al. 2009](#)) suggesting the possibility of relatively recent (Gyr) galaxy mergers. If a galaxy nucleus contains a binary SMBH then 3-body scattering will gradually harden their orbit to a pc-scale separation, while ejecting many stars and incurring tidal disruptions more often than a single central object would (e.g. [Quinlan 1996](#); [Ivanov, Polnarev & Saha 2005](#); [Chen et al. 2009, 2011](#); [Wegg & Nate Bode 2011](#)). A significantly non-spherical stellar background potential could also increase the TDE rate ([Vasiliev 2014](#)). Since SMBH binaries and asymmetric morphologies are both expected outcomes of galaxy mergers, it

<sup>3</sup> We use the scaling of  $T_{\text{gas}} \sim 10^5 \text{ K}$  in eq. (16), as it is roughly the thermodynamic equilibrium  $T$  of gas that is located at a distance  $R_c$  from a continuum source with  $T_{\text{BB}} = T_i \sim 10^9 \text{ K}$ , i.e.  $T_{\text{gas}} \approx T_i \sqrt{R_i/R_c}$  (see eq. 7).

may be that the overabundance of TDE-candidates in these galaxies is related to their relatively recent galaxy merger history. However, the expected increased rates are typically at most a few times larger, while the inferred rates in such galaxies appear to be at least an order of magnitude (if not more) larger than expected given the rarity of E+A galaxies: only as few as  $\lesssim 10^{-2}$  of all galaxies (Zabludoff et al. 1996; Goto et al. 2003; Quintero et al. 2004; Vergani et al. 2010).

Some E+A galaxies seem to feed low-luminosity AGN (Yang et al. 2006), and the evidence of an intermediate (Gyr ago) star-formation epoch suggests the existence of gas reservoir, which is lower than star-forming galaxies, but can be sufficient for a spasmodic, low rate feeding of an AGN, potentially producing starved/subluminous AGNs. If the TDE-candidate flares are not bona-fide TDEs but are related to bursts from subluminous AGNs (a possibility discussed in the next section), then such E+A galaxies might indeed provide favourable conditions, and explain why such nuclear flares preferentially reside in E+A hosts.

### 3.3 Alternative (non TDE) origins for TDE-candidates

#### 3.3.1 A nuclear supernova

While the continuum source of TDE candidates may be explained by a (super-luminous) SN explosion, the required density of line-emitting gas ( $n_{\text{gas}} \sim 10^{12} \text{ cm}^{-3}$ ) is large compared to the densities expected for the ISM of quiescent galaxies. Such a large  $n_{\text{gas}}$  is typical of the nuclear region of AGN (e.g. Netzer 2013). French, Arcavi & Zabludoff (2016) report that detections are preferentially found in Balmer-strong galaxies, i.e. galaxies that recently have had a strong starburst (roughly within the last Gyr). A strong starburst requires a large supply of gas, a fraction of which may as well reach the host nucleus and feed an AGN. This activity quenches star formation in the nuclear region; the only exception is the dusty torus where starbursts may occur continuously throughout the life of AGN (Collin & Zahn 1999a,b; Sirko & Goodman 2003). Thus, a candidate TDE may be the SN explosion of a progenitor star that formed locally within the torus. The explosion occurs shortly after the nucleus becomes dormant ( $\lesssim 10^3$  yr), before the dense clumps of gas disperse (or collapse). An AGN has a life-time of  $\sim 10^8$  yr. A star of a few  $10m_{\odot}$  lives for a few  $10^7$  yr. Thus, the expected fraction of TDE candidates in quiescent Balmer-strong galaxies is  $\sim 10^7/10^8 = 10\%$ , consistent with observations (French, Arcavi & Zabludoff 2016). TDE candidates that do not pass through a He II-bright phase, may be SN explosions in a nucleus that no longer has dense enough clumps. A model of gas with  $\tau_{\text{rec}} > \tau_{\text{var}}$  requires non-equilibrium photoionization calculations, and is beyond the scope of this study. This scenario naturally explains the observed emission-line width of a few  $1000 \text{ km s}^{-1}$  in TDE candidates, which is typical of the (broad) emission-line region of AGN.

The SN-explosion scenario for TDE candidates may also explain the peculiar SNe of type II-L and II-P, which exhibit spectral behaviour similar to He II-bright TDE candidates (Smith et al. 2015). These are likely SN explosions of massive progenitors that detonate near a reservoir of dense gas (e.g. protostellar clouds). A possible connection between

TDE candidates and extreme SN explosions was previously pointed out by others (Komossa et al. 2009; Drake et al. 2011). Here, we establish this connection from photoionization considerations. Gezari et al. (2009) disfavour the connection, pointing out that the UV continuum emission (i.e.  $T_{\text{BB}} \gtrsim 10^4 \text{ K}$ ) fades significantly faster in SNe compared to TDE candidates (weeks versus months). This discrepancy may be explained by a denser ISM that is expected in a galactic nucleus. The denser ISM is likely to slow the cooling of SN ejecta, and to produce a shallower light-curve for SNe in the nucleus. Finally, we note that similar connections between nuclear SNe and AGN activity has been suggested in the literature before (e.g. Terlevich et al. 1992; Aretxaga & Terlevich 1994; Ulrich, Maraschi & Urry 1997; Aretxaga 1999); but extending this possibility in the context of singular TDE-candidate events, is more attractive compared to the previously suggested connection to recurrent AGN activity and flaring.

#### 3.3.2 Subluminous AGN flaring scenario

Another alternative possibility is that the UV/O TDE candidates could have been a type of unrecognized flaring from accretion onto a MBH, possibly in a subluminous/starved AGN that lacks strong emission line regions during a long semi-quiescent state. Circumnuclear clouds may be present, but normally not irradiated strongly enough for an observable BLR (or NLR). Some transient hosts may be senescent or starving AGN, which have already accreted most of the available interstellar gas. These could be related to AGNs that change their BLR type and/or missing them (e.g. Tran 2001; Bianchi et al. 2005; Zhang & Wang 2006; Kaastra et al. 2014), which can occur even on short timescales (Storchi-Bergmann, Baldwin & Wilson (1993); Aretxaga (1999); Shappee et al. (2014); Oknyansky et al. (2016). Some peculiar types of AGNs can play a similar role, e.g. XBONG sources (Elvis et al. 1981; Griffiths et al. 1995; Comastri et al. 2002; Fiore et al. 2003; Severgnini et al. 2003; a few of which are E+A galaxies Kim et al. 2006). In particular, variability in blazars and BL Lac objects can exceed several optical magnitudes (Eggen 1973; Xie et al. 2002; Dolcini et al. 2005; Danforth et al. 2013; Sandrinelli, Covino & Treves 2014).

Indeed, there are a few possible examples. Campana et al. (2015) proposed a reverse argument — explaining recurrent AGN flaring in the weak AGN in IC 3599. Alloin et al. (1986) observe recurrent outbursts in a low-powered AGN, each of which behaved like an intermediate phenomenon between modern TDE candidates and the normal activity of a steady AGN, while Saxton et al. (2015) suggested to relate a transient TDE-like event to a disc instability around a weak AGN in NGC 3599.

Flaring might be fed by an episodic surge of accretion: a disc instability, an abrupt change in accretion state, or passage of a massive object through the disc. Accretion might increase if a new gas source arrives, derived from a cloud that has scattered into a diving orbit, much like the disruption of a self-bound star. Whatever the trigger and the fuel, flaring then excites one or more previously dormant circumnuclear clouds; if they cover enough of the nucleus then the result is a transient BLR. One then still needs to explain the lack of hard radiation from the inner parts of the disc. This may

occur if a cavity exists in the inner region. Laor (2003) proposed that shear destroys any BLR clouds within a limiting orbital radius, but the number of clouds irradiated enough to emit the broad lines depends on the central luminosity. Consequently, an AGN weaker than some threshold will not have any observable BLR. It is therefore conceivable that a nuclear *brightening* in a previously *unrecognised* AGN can activate previously unilluminated BLR clouds, giving the false appearance of a TDE. This depends on the weakness of ordinary AGN signatures in the initial state.

Among conceivable types of peculiar flaring from NBHs, the disc-instability model of Kim (2010) might be extended from microquasars to instability in a disc around a MBH. In this case, an instability in the inner accretion disc can lead to draining of the inner region, producing an inner cavity, while the accreted material powers a flare. The flaring can later be echoed by more distant material, as described in the echo model. Given the observational selection bias against AGN hosts, such events are likely to be identified only in cases where a gaseous disc exists around a MBH, but the accretion is not sufficient to power an observable AGN, e.g. in cases of starved or subluminescent AGNs, where circumnuclear gas exist, but is scarce. These might possibly correspond to E+A galaxies, in which star-formation and hence gas supply were abundant in the relatively near (but not recent) past, while the MBH now feeds only on the late and little infalling gas following the past merger event. Even drier galaxies would not have sufficient supply, and the MBH would not sustain a disc in which instabilities could occur.

Another model by Tanaka (2013) involving binary MBH may also be relevant. A binary SMBH clears a central cavity in its accretion disc, which appears dimmer and softer than an equivalent single-AGN disc. Depending on the binary period, intermittent gas streams of perhaps  $0.1m_{\odot}$  dive towards the SMBHs from the cavity's lip. Each stream shocks near the recipient SMBH, causing a flare resembling a TDE. If the recurrence period is long compared to the modern era of transient monitoring, then a single detection could be misidentified as a TDE. The recurrence period, debris velocities and energy yields in a cavity flare depend on the binary separation, and need not correspond to predicted tidal radii of stellar disruptions. Binary cavity flares might be distinguished by subtle details: the steepness of their fading, or by their occurrence around a SMBH that is too massive for a TDE. (For example, Leloudas et al. 2016 recently infer  $m_{\bullet} > 10^8 m_{\odot}$  in the weak-lined TDE candidate ASASSN-15lh.) If SMBH binaries are a common product of the mergers that create E+A galaxies, then the cavity flare mechanism might explain the peculiar incidence of UV/O nuclear transients in these hosts.

Let us consider generically what happens as the amplitude of an AGN flare is increased (whether it is a coincidence of jet internal shocks, or an accretion surge due to disc instability). For a small-amplitude event, the rising and the fading involve similar physics, and phenomena are almost reversible in time. A more luminous flash exerts an impulsive radiation pressure on opaque circumnuclear clouds (if dense enough). At greater intensities, the peak luminosity exceeds the local Eddington limit, driving a radiation-dominated outflow, which could in turn drive external shocks into the ISM, resulting in a prolonged, fading afterglow like those of gamma-ray bursts. The emergent luminosity is limited to a few times

$L_E$ , but a radiation-driven wind could carry more kinetic power. Thus an asymmetry between rising and fading rates is naturally expected for higher-amplitude events.

If the energy injection is abrupt and intense enough to propel an *opaque* radiation-dominated explosion then the responsible process is concealed. In super-Eddington models, the wind photosphere conceals the accretion disc and central object. This explains why late-time UV/O candidate temperatures are a few times  $10^4\text{K}$ , rather than the  $10^5\text{K}$  temperatures expected for disc material near the tidal radius (e.g. Jaroszynski, Abramowicz & Paczynski 1980; Loeb & Ulmer 1997; Ulmer 1999). This generic self-concealment of super-Eddington events implies that a high-amplitude AGN outburst may be practically difficult to distinguish from a TDE flare, or an unusual supernova detonating in a dense medium (Smith et al. 2015). The radio, X-ray and  $\gamma$ -ray components of some TDE candidates could be the result of collimated jets erupting through the opaque surface: briefly, persistently, or with instabilities and precession effects depending on idiosyncrasies of each system (e.g. Gezari et al. 2009; van Velzen, K rding & Falcke 2011; Bloom et al. 2011; Levan et al. 2011; van Velzen et al. 2013; Saxton et al. 2012; Cenko et al. 2012b; Bower et al. 2013; van Velzen et al. 2016a; Alexander et al. 2016). In events where jets ceased after an initial burst, it is conceivable that their emissions might ionize distant clouds, similarly to the early high-energy ‘flash’ in our light-echo models.

## 4 CONCLUSIONS

In this study we explored the spectral features of tidal disruption event candidates. Our analysis shows that none of the models currently used can explain both the origin of the line ratios as well as the individual equivalent widths seen in observations. We find that models of blackbody illumination could yield realistic line emissions, but only when considering a hot source ( $10^6\text{K}$ ), while a  $10^4\text{K}$  blackbody is consistent with the continuum observed in UV/O TDE candidates. We propose a novel light-echo model that can resolve these difficulties, and has important implications for the early evolution of the explosive event and the later temporal evolution of the spectral features. In the light-echo model, an initial hard radiation flash illuminates BLR clouds residing at distances on the order of ten light-days. Their strong line emission is then seen superimposed on the softened nuclear spectrum emitted at a later time. Our model can therefore provide a prediction that TDE candidates should appear X-ray bright concurrently with the HeII state and earlier, but much fainter in X-rays after tens of days later. This modelling is generic to near-super-Eddington outbursts in a galaxy nucleus, as long as there are some nearby clouds with  $n_{\text{H}} \sim 10^{12}\text{cm}^{-3}$ . It is difficult to distinguish between a tidal disruption event, an outburst by an impoverished AGN, or an exotic superluminous supernova in this context, or perhaps other explosive events not yet recognized.

A weak AGN accreting at a low average rate, with a nearly exhausted gas supply, might mimic a TDE if a high-amplitude flare photoionizes the few clouds of a normally dim and impoverished BLR. The He-overbright state can occur in the BLR of a semi-starved AGN. If the event is an AGN flare illuminating an unevolving cloud system, on

bound orbits, then the occurrence of a He-overbright state depends on the presence of a cloud population with densities in the critical range  $10^{11} < n_{\text{H}} < 10^{13} \text{ cm}^{-3}$ . If such a system reveals the He-overbright state at all, then it might happen twice: once while  $\Phi_{\text{H}}$  is rising and again during the fall. If however the transient event involves ballistically or dynamically expanding debris, then the He-overbright state might occur only once. In future, higher-cadence transient monitoring and spectroscopy will test these possibilities.

## ACKNOWLEDGEMENTS

We thank Ari Laor, Iair Arcavi and Shai Kaspi for helpful discussions. This work has made use of NASA's Astrophysics Data System. Calculations were performed with version 13.03 of CLOUDY, last described by Ferland et al. (2013). This publication has made use of code written by James R. A. Davenport.<sup>4</sup> Specifically, the figure color scheme<sup>5</sup> was developed by Green (2011). CJS and HBP acknowledge support from the Israel Science Foundation through the astrophysics I-CORE program 1829/12. CJS thanks D.M.Greer, R. & R. Whittaker for their hospitality during this work.

## REFERENCES

- Alexander K. D., Berger E., Guillochon J., Zauderer B. A., Williams P. K. G., 2016, *ApJ*, 819, L25
- Alloin D., Pelat D., Phillips M. M., Fosbury R. A. E., Freeman K., 1986, *ApJ*, 308, 23
- Arcavi I. et al., 2014, *ApJ*, 793, 38
- Aretxaga I., 1999, in *IAU Symposium*, Vol. 193, *Wolf-Rayet Phenomena in Massive Stars and Starburst Galaxies*, van der Hucht K. A., Koenigsberger G., Eenens P. R. J., eds., p. 716
- Aretxaga I., Terlevich R., 1994, *MNRAS*, 269, 462
- Baldwin J., Ferland G., Korista K., Verner D., 1995, *ApJ*, 455, L119
- Baskin A., Laor A., Stern J., 2014, *MNRAS*, 438, 604
- Bianchi S., Guainazzi M., Matt G., Chiaberge M., Iwasawa K., Fiore F., Maiolino R., 2005, *A&A*, 442, 185
- Blandford R. D., McKee C. F., 1976, *Physics of Fluids*, 19, 1130
- Bloom J. S. et al., 2011, *Science*, 333, 203
- Bower G. C., Metzger B. D., Cenko S. B., Silverman J. M., Bloom J. S., 2013, *ApJ*, 763, 84
- Brown M. J. I. et al., 2009, *ApJ*, 703, 150
- Campana S., Mainetti D., Colpi M., Lodato G., D'Avanzo P., Evans P. A., Moretti A., 2015, *A&A*, 581, A17
- Cenko S. B. et al., 2012a, *MNRAS*, 420, 2684
- Cenko S. B. et al., 2016, *ApJ*, 818, L32
- Cenko S. B. et al., 2012b, *ApJ*, 753, 77
- Chen X., Madau P., Sesana A., Liu F. K., 2009, *ApJ*, 697, L149
- Chen X., Sesana A., Madau P., Liu F. K., 2011, *ApJ*, 729, 13
- Chornock R. et al., 2014, *ApJ*, 780, 44
- Cohen E., Piran T., 1999, *ApJ*, 518, 346
- Collin S., Zahn J.-P., 1999a, *A&A*, 344, 433
- Collin S., Zahn J.-P., 1999b, *Ap&SS*, 265, 501
- Comastri A. et al., 2002, *ApJ*, 571, 771
- Danforth C. W., Nalewajko K., France K., Keeney B. A., 2013, *ApJ*, 764, 57
- Dolcini A. et al., 2005, *A&A*, 443, L33
- Dong S. et al., 2016, *Science*, 351, 257
- Dou L., Wang T.-g., Jiang N., Yang C., Lyu J., Zhou H., 2016, *ArXiv e-prints*, 1605.05145
- Drake A. J. et al., 2011, *ApJ*, 735, 106
- Dressler A., Gunn J. E., 1983, *ApJ*, 270, 7
- Eddington A. S., 1918, *ApJ*, 48, 205
- Eggen O. J., 1973, *ApJ*, 186, L1
- Elvis M., Schreier E. J., Tonry J., Davis M., Huchra J. P., 1981, *ApJ*, 246, 20
- Ferland G. J. et al., 2013, *Rev.Mex.AA*, 49, 137
- Fiore F. et al., 2003, *A&A*, 409, 79
- Frank J., Rees M. J., 1976, *MNRAS*, 176, 633
- French K. D., Arcavi I., Zabludoff A., 2016, *ApJ*, 818, L21
- Gal-Yam A., 2012, *Science*, 337, 927
- Gaskell C. M., Rojas Lobos P. A., 2014, *MNRAS*, 438, L36
- Generozov A., Mimica P., Metzger B. D., Stone N. C., Giannios D., Aloy M. A., 2017, *MNRAS*, 464, 2481
- Gezari S. et al., 2008, *ApJ*, 676, 944
- Gezari S., Chornock R., Lawrence A., Rest A., Jones D. O., Berger E., Challis P. M., Narayan G., 2015, *ApJ*, 815, L5
- Gezari S. et al., 2012, *Nature*, 485, 217
- Gezari S. et al., 2009, *ApJ*, 698, 1367
- Goel A., Maity R., Roy P., Sarkar T., 2015, *Phys. Rev. D*, 91, 104029
- Goto T., Kawai A., Shimono A., Sugai H., Yagi M., Hattori T., 2008, *MNRAS*, 386, 1355
- Goto T. et al., 2003, *PASJ*, 55, 771
- Green D. A., 2011, *Bulletin of the Astronomical Society of India*, 39, 289
- Griffiths R. E., Georgantopoulos I., Boyle B. J., Stewart G. C., Shanks T., della Ceca R., 1995, *MNRAS*, 275, 77
- Guillochon J., Manukian H., Ramirez-Ruiz E., 2014, *ApJ*, 783, 23
- Guillochon J., Ramirez-Ruiz E., 2013, *ApJ*, 767, 25
- Guillochon J., Ramirez-Ruiz E., 2015, *ApJ*, 809, 166
- Gurzadian V. G., Ozernoi L. M., 1981, *A&A*, 95, 39
- Hills J. G., 1975, *Nature*, 254, 295
- Holoien T. W.-S. et al., 2016a, *MNRAS*, 463, 3813
- Holoien T. W.-S. et al., 2016b, *MNRAS*, 455, 2918
- Holoien T. W.-S. et al., 2014, *MNRAS*, 445, 3263
- Inserra C., et al., 2013, *ApJ*, 770, 128
- Ivanov P. B., Polnarev A. G., Saha P., 2005, *MNRAS*, 358, 1361
- Jaroszynski M., Abramowicz M. A., Paczynski B., 1980, *Acta Astron.*, 30, 1
- Jiang N., Dou L., Wang T., Yang C., Lyu J., Zhou H., 2016, *ApJ*, 828, L14
- Kaasra J. S. et al., 2014, *Science*, 345, 64
- Kaspi S., Maoz D., Netzer H., Peterson B. M., Vestergaard M., Jannuzi B. T., 2005, *ApJ*, 629, 61
- Kato M., Hōshi R., 1978, *Progress of Theoretical Physics*, 60, 1692
- Kewley L. J., Geller M. J., Barton E. J., 2006, *AJ*, 131, 2004
- Kim D.-W. et al., 2006, *ApJ*, 644, 829
- Kim S.-W., 2010, *Journal of Korean Physical Society*, 57, 673
- Komossa S., 2015, *Journal of High Energy Astrophysics*, 7, 148
- Komossa S. et al., 2009, *ApJ*, 701, 105
- Korista K. T., Goad M. R., 2004, *ApJ*, 606, 749
- Lacy J. H., Townes C. H., Hollenbach D. J., 1982, *ApJ*, 262, 120
- Laor A., 2003, *ApJ*, 590, 86
- Laor A., Fiore F., Elvis M., Wilkes B. J., McDowell J. C., 1997, *ApJ*, 477, 93
- Leloudas G. et al., 2016, *ArXiv e-prints*
- Levan A. J. et al., 2011, *Science*, 333, 199
- Lidskii V. V., Ozernoi L. M., 1979, *Soviet Astronomy Letters*, 5, 16
- Lodato G., King A. R., Pringle J. E., 2009, *MNRAS*, 392, 332
- Loeb A., Ulmer A., 1997, *ApJ*, 489, 573
- Luminet J.-P., Marck J.-A., 1985, *MNRAS*, 212, 57
- Mathews W. G., Ferland G. J., 1987, *ApJ*, 323, 456

<sup>4</sup> <http://www.astro.washington.edu/users/jrad/id1.html>

<sup>5</sup> <http://www.mrao.cam.ac.uk/~dag/CUBEHELIX/>

Meliani Z., Vincent F. H., Grandclément P.,ourgoulhon E., Monceau-Baroux R., Straub O., 2015, *Classical and Quantum Gravity*, 32, 235022

Miller J. M. et al., 2015, *Nature*, 526, 542

Netzer H., 2013, *The Physics and Evolution of Active Galactic Nuclei*

Oknyansky V. L. et al., 2016, *The Astronomer's Telegram*, 9015

Ozernoi L. M., Reinhardt M., 1978, *Ap&SS*, 59, 171

Perets H. B., Li Z., Lombardi, Jr. J. C., Milcarek, Jr. S. R., 2016, *ApJ*, 823, 113

Piran T., Svirski G., Krolik J., Cheng R. M., Shiohawa H., 2015, *ApJ*, 806, 164

Pracy M. B., Kuntschner H., Couch W. J., Blake C., Bekki K., Briggs F., 2009, *MNRAS*, 396, 1349

Pracy M. B., Owers M. S., Zwaan M., Couch W., Kuntschner H., Croom S. M., Sadler E. M., 2014, *MNRAS*, 443, 388

Quinlan G. D., 1996, *New Astronomy*, 1, 35

Quintero A. D. et al., 2004, *ApJ*, 602, 190

Rees M. J., 1988, *Nature*, 333, 523

Renzini A., Greggio L., di Serego Alighieri S., Cappellari M., Burstein D., Bertola F., 1995, *Nature*, 378, 39

Roth N., Kasen D., Guillochon J., Ramirez-Ruiz E., 2016, *ApJ*, 827, 3

Sandrinelli A., Covino S., Treves A., 2014, *A&A*, 562, A79

Saxton C. J., Soria R., Wu K., Kuin N. P. M., 2012, *MNRAS*, 422, 1625

Saxton C. J., Younsi Z., Wu K., 2016, *MNRAS*, 461, 4295

Saxton R. D., Motta S. E., Komossa S., Read A. M., 2015, *MNRAS*, 454, 2798

Severgnini P. et al., 2003, *A&A*, 406, 483

Shappee B. J. et al., 2014, *ApJ*, 788, 48

Sirko E., Goodman J., 2003, *MNRAS*, 341, 501

Smith N. et al., 2015, *MNRAS*, 449, 1876

Storchi-Bergmann T., Baldwin J. A., Wilson A. S., 1993, *ApJ*, 410, L11

Strubbe L. E., Murray N., 2015, *MNRAS*, 454, 2321

Strubbe L. E., Quataert E., 2009, *MNRAS*, 400, 2070

Svirski G., Piran T., Krolik J., 2015, *ArXiv e-prints*, 1508.02389

Tanaka T. L., 2013, *MNRAS*, 434, 2275

Terlevich R., Tenorio-Tagle G., Franco J., Melnick J., 1992, *MNRAS*, 255, 713

Tran H. D., 2001, *ApJ*, 554, L19

Ulmer A., 1999, *ApJ*, 514, 180

Ulrich M.-H., Maraschi L., Urry C. M., 1997, *ARA&A*, 35, 445

van Velzen S. et al., 2016a, *Science*, 351, 62

van Velzen S. et al., 2011, *ApJ*, 741, 73

van Velzen S., Frail D. A., Körding E., Falcke H., 2013, *A&A*, 552, A5

van Velzen S., Körding E., Falcke H., 2011, *MNRAS*, 417, L51

van Velzen S., Mendez A. J., Krolik J. H., Gorjian V., 2016b, *ApJ*, 829, 19

Vasiliev E., 2014, *Classical and Quantum Gravity*, 31, 244002

Vergani D. et al., 2010, *A&A*, 509, A42

Verner D. A., Ferland G. J., 1996, *ApJS*, 103, 467

Vreeswijk P. M., et al., 2014, *ApJ*, 797, 24

Wang T.-G., Zhou H.-Y., Wang L.-F., Lu H.-L., Xu D., 2011, *ApJ*, 740, 85

Wegg C., Nate Bode J., 2011, *ApJ*, 738, L8

Wyrzykowski L. et al., 2016, *ArXiv e-prints*, 1606.03125

Xie G. Z., Liang E. W., Xie Z. H., Dai B. Z., 2002, *AJ*, 123, 2352

Yamauchi C., Goto T., 2005, *MNRAS*, 359, 1557

Yang Y., Tremonti C. A., Zabludoff A. I., Zaritsky D., 2006, *ApJ*, 646, L33

Yang Y., Zabludoff A. I., Zaritsky D., Lauer T. R., Mihos J. C., 2004, *ApJ*, 607, 258

Young P. J., Shields G. A., Wheeler J. C., 1977, *ApJ*, 212, 367

Zabludoff A. I., Zaritsky D., Lin H., Tucker D., Hashimoto Y., Shectman S. A., Oemler A., Kirshner R. P., 1996, *ApJ*, 466,

104

Zel'dovich Y. B., Raizer Y. P., 1967, *Physics of shock waves and high-temperature hydrodynamic phenomena*

Zhang E.-P., Wang J.-M., 2006, *ApJ*, 653, 137

## APPENDIX A: CURRENTLY IDENTIFIED O/UV TDE CANDIDATES

Table A1 provides a listing of currently identified TDE candidate events with spectral lines, including the transient previously identified by Drake et al. (2011) as a SN (but see Generozov et al. 2017 suggesting it is too luminous for a TDE). The clouds' emission line characteristic velocity ( $v$ ) is defined as in Arcavi et al. (2014). Where the observational papers give a bolometric luminosity ( $L$ ), we use those values. Otherwise, we interpolate and estimate values from the published photometric light-curves.

Through dimensional analyses, it can be shown that the composite scores  $v^4/L$  and  $Lv^4/m_\bullet$  should be correlated with ionization parameter (if details of the system geometry were otherwise equal). In these terms, there seems to be a tendency for the H $\alpha$ -bright events to have lower scores than the He II-overbright events. It is however not a strong trend, and perhaps not statistically significant. We were unable to use Table A1 to declare any clear, quantitative predictor of the Arcavi et al. (2014) spectral sequence. In the Appendix B, we search for patterns and discriminants in a different way, under particular model assumptions.

## APPENDIX B: OBSERVED VS EXPECTED VELOCITIES OF THE ILLUMINATED CLOUD

The presently available observations ought to appear more orderly under assumption of an event type: TDE or AGN flare. Empirically, the characteristic radius of a steady active galaxy's BLR is  $R_{\text{BLR}} \approx R_{44}(L/10^{44} \text{ erg s}^{-1})^A$  where an index  $A = \frac{1}{2}$  is the ideal if the BLR size were constrained by a threshold temperature (e.g. of dust sublimation). From reverberation mapping in the 5100Å monochromatic luminosity  $\lambda L_\lambda$ , Kaspi et al. (2005) find  $R_{44} = 22.3 \pm 2.1$  light day and  $A = 0.69 \pm 0.05$ . Given this sizing, and SMBH mass estimates (Arcavi et al. 2014), we obtain a characteristic orbital velocity of the BLR clouds ( $v_k$ ). If however the event were a TDE, then the stellar tidal disruption radius provides the relevant  $v_k$  estimator. Fig. B1 compares observed spectroscopic line widths ( $v_s$ ) to the  $v_k$  estimates in both models. Assuming stars of solar density, the TDE scenario works poorly: the measured velocities are 0.02 to 0.2 times predicted, and the values seem uncorrelated with  $v_k$ ; and neither does the AGN model show any significant correlation. The measured velocities are a factor of a few higher than AGN expectations. From these simple scaling arguments, neither the TDE nor AGN scenarios fits the UV/O events impressively well, but the AGN version may seem somewhat less discordant. The weakness of the correlation between actual and expected velocities implies that the line-emitters are not causally related to the flaring event. Rather, we suppose that they were pre-existing, dormant circumnuclear clouds that revived and reactivated as a BLR when irradiated by the explosive event.

**Table A1.** Column 1: name of the TDE event or host. Column 2: type of broad line system: He-dominated emission; both HeII and H $\alpha$  emission; H $\alpha$ -dominated emission; absorption. Column 3: SMBH mass estimate. Column 4: time relative to peak luminosity. column 5: blackbody temperature (alternative versions for PS1-10jh). Column 6: photometry used ('-' marks bolometric estimates given by reference). Column 7: luminosity (derived from photometry if necessary). Column 8: velocity width of broad line. Column 9: ionization estimator using estimated  $m_{\bullet}$ . Column 11: references: (a) Gezari et al. 2012; (b) Arcavi et al. 2014; (c) Wang et al. 2011; (d) Holoien et al. 2014; (e) van Velzen et al. 2011; (f) Drake et al. 2011; (g) Chornock et al. 2014; (h) Miller et al. 2015; (i) Holoien et al. 2016b; (j) Holoien et al. 2016a; (k) Wyrzykowski et al. 2016.

object	type	$m_{\bullet}$ ( $10^6 m_{\odot}$ )	$t$ (day)	$T_{\text{bb}}$ ( $10^4$ K)	band	$L$ ( $10^9 L_{\odot}$ )	$v$ ( $10^3$ km/s)	$\log\left(\frac{v^4}{L}\right)$	$\log\left(\frac{Lv^4}{m_{\bullet}^2}\right)$	ref.
PS1-10jh	He	$4.0_{-2}^{+4}$	-22	$\gtrsim 2.9 \pm 0.2$	$g_{P1} r_{P1} i_{P1}$	$\gtrsim 22.6 \pm 3$	$5.43 \pm 1.46$	$\lesssim 1.6 \pm 1.1$	$\gtrsim 3.1_{-1.5}^{+2.3}$	a,b
PTF09ge	He	$5.65_{-0.98}^{+3.02}$	-18	$2.1 \pm 0.3$	-	$13.0 \pm 4.6$	$10.07 \pm 0.67$	$2.9 \pm 0.4$	$3.6_{-0.6}^{+1.2}$	b
SDSSJ0748	He+H	$11.78_{-3.56}^{+2.29}$	> 0	$1.3 \pm 0.4$	$g$	$1.4 \pm 0.6$	$9.95 \pm 0.51$	$3.8 \pm 0.5$	$2.0_{-0.8}^{+0.6}$	b,c
ASASSN-14ae	H	$2.45_{-0.74}^{+1.55}$	0	$2.3 \pm 0.1$	$V$	$38.3 \pm 3.6$	$3.60 \pm 0.18$	$0.6 \pm 0.2$	$3.0_{-0.6}^{+1.3}$	b,d
	H	..	4	$2.1 \pm 0.1$	-	$10.5 \pm 0.4$	$7.2 \pm 0.2$	$2.4 \pm 0.1$	$3.7_{-0.6}^{+1.3}$	
	H	..	30	$1.6 \pm 0.1$	-	$5.6 \pm 0.4$	$6.0 \pm 0.2$	$2.4 \pm 0.2$	$3.1_{-0.6}^{+1.3}$	
	H	..	51	$1.6 \pm 0.1$	-	$2.9 \pm 0.2$	$5.1 \pm 0.2$	$2.4 \pm 0.2$	$2.5_{-0.6}^{+1.3}$	
	H	..	73	$2.1 \pm 0.2$	-	$1.7 \pm 0.2$	$4.2 \pm 0.2$	$2.3 \pm 0.2$	$2.0_{-0.6}^{+1.3}$	
	He+H	..	94	$2.1 \pm 0.3$	-	$1.3 \pm 0.3$	$3.4 \pm 0.2$	$2.0 \pm 0.3$	$1.5_{-0.7}^{+1.3}$	
	He+H	..	132	$2.0 \pm 0.2$	-	$0.3 \pm 0.2$	$3.4 \pm 0.2$	$2.6 \pm 0.6$	$0.8_{-0.9}^{+1.4}$	
ASASSN-15oi	He	$25.0_{-13}^{+25}$	7	$2.0 \pm 0.4$	-	$52.0 \pm 25$	$8.4 \pm 0.4$	$2.0 \pm 0.5$	$2.6_{-1.1}^{+2.1}$	j
	He+H	..	21	$7.5 \pm 0.4$	-	$35.0 \pm 17$	$3.9 \pm 0.4$	$0.8 \pm 0.6$	$1.1_{-1.2}^{+2.1}$	
ASASSN-14li	He+H	$3.0 \pm 2$	35	$3.5 \pm 0.4$	-	$83.2 \pm 2.6$	$1.3 \pm 0.4$	$-1.5 \pm 1.3$	$1.4 \pm 1.9$	h,i
OGLE16aaa	He+H	$3.8_{-1.9}^{+3.8}$	-3	$\gtrsim 2.2$	$I$	$86.0 \pm 4$	$7.6 \pm 0.4$	$1.6 \pm 0.2$	$4.3_{-1.0}^{+2.0}$	k
PTF09axc	H	$2.69_{-0.64}^{+0.66}$	$\approx 5$	$1.2 \pm 0.2$	-	$4.7 \pm 2.4$	$11.89 \pm 0.22$	$3.6 \pm 0.5$	$4.1 \pm 0.7$	b
PTF09djl	H	$3.57_{-2.96}^{+9.97}$	2	$2.6 \pm 0.4$	-	$30.0 \pm 14$	$6.53 \pm 0.35$	$1.8 \pm 0.5$	$3.6_{-1.7}^{+5.6}$	b
		..	31	$2.0 \pm 0.3$	-	$15.0 \pm 9$	$6.53 \pm 0.35$	$2.1 \pm 0.6$	$3.3_{-1.7}^{+5.6}$	
		..	62	$> 3.2$	-	$< 124$	$6.53 \pm 0.35$	$> 1.2 \pm 0.2$	$< 4.2_{-1.7}^{+5.6}$	
TDE2	H	$35.52_{-25.80}^{+55.31}$	> 40	$1.82 \pm 0.07$	$g$	$42.0 \pm 2.9$	$3.44 \pm 0.11$	$0.5 \pm 1.3$	$0.7_{-1.9}^{+3.4}$	b,e
CSS100217	H	$14.7_{-2.0}^{+2.4}$	-5	$1.62 \pm 0.18$	$V$	$439.0 \pm 104$	$1.20 \pm 0.04$	$-2.3 \pm 0.3$	$0.6 \pm 0.3$	f
		..	20	$1.35 \pm 0.08$	$V$	$267.0 \pm 36$	$1.36 \pm 0.04$	$-1.9 \pm 0.2$	$0.6_{-0.3}^{+0.4}$	
		..	84	$0.78 \pm 0.20$	$V$	$67.0 \pm 16$	$2.07 \pm 0.04$	$-0.6 \pm 0.3$	$0.6 \pm 0.5$	
		..	164		$V$	$< 4.6 \pm 1.1$	$1.63 \pm 0.04$	$> 0.2 \pm 0.3$	$< -1.0 \pm 0.6$	
PS1-11af	abs	$8.0 \pm 2.0$	24	$1.7 \pm 0.3$	-	$22.1 \pm 0.5$	$4.31 \pm 0.34$	$1.2 \pm 0.3$	$1.9 \pm 0.3$	g

### APPENDIX C: CLOUDY CALCULATIONS AND THE LINE RATIOS IN THE PHOTOIONIZATION CUBE PARAMETER PHASE SPACE

For each SED, we run several cubes of calculations: exploring a rectangle of ( $N_{\text{H}}, n_{\text{H}}, \Phi_{\text{H}}$ ) in steps of 0.1 dex, and saving depth profiles along the  $N_{\text{H}}$  or spatial axis. For greater resolution, and to check consistency, we rerun extra cubes where the maximum column was set to  $N_{\text{H}} = 10^{23}, 10^{24}, 10^{25} \text{ cm}^{-2}$ . In every numerical run, CLOUDY reports the mean energy of a photoionizing photon (**Average nu**), the intensity of ionizing photons (**I(nu>1ryd)**), and the total intensity (**Total inten**). Using these, or numerical integration of the known SED function, provides a characteristic photon energy ( $\bar{\epsilon}$ ,

enabling conversion between the ionizing flux ( $\Phi_{\text{H}}$ , user selected), an assumed cloud radial position ( $R_{\text{c}}$ ), and the bolometric luminosity of the source ( $L$ ). If  $L$  is known, then we infer the distance between the central source and the photoionized cloud,

$$R_{\text{c}} = \left[ \frac{L}{4\pi\bar{\epsilon}\Phi_{\text{H}}} \right]^{1/2}. \quad (\text{C1})$$

The emission line luminosity ( $L_{\lambda}$ ) and the cloud mass ( $M_{\text{c}}$ ) depend on the cloud covering factor ( $0 < \Omega < 1$ ) and the specific intensity of the line ( $I_{\lambda}$ , calculated by CLOUDY). We generally have

$$L_{\lambda} = 4\pi R_{\text{c}}^2 I_{\lambda} \Omega = \frac{L}{\bar{\epsilon}\Phi_{\text{H}}} I_{\lambda} \Omega \quad (\text{C2})$$

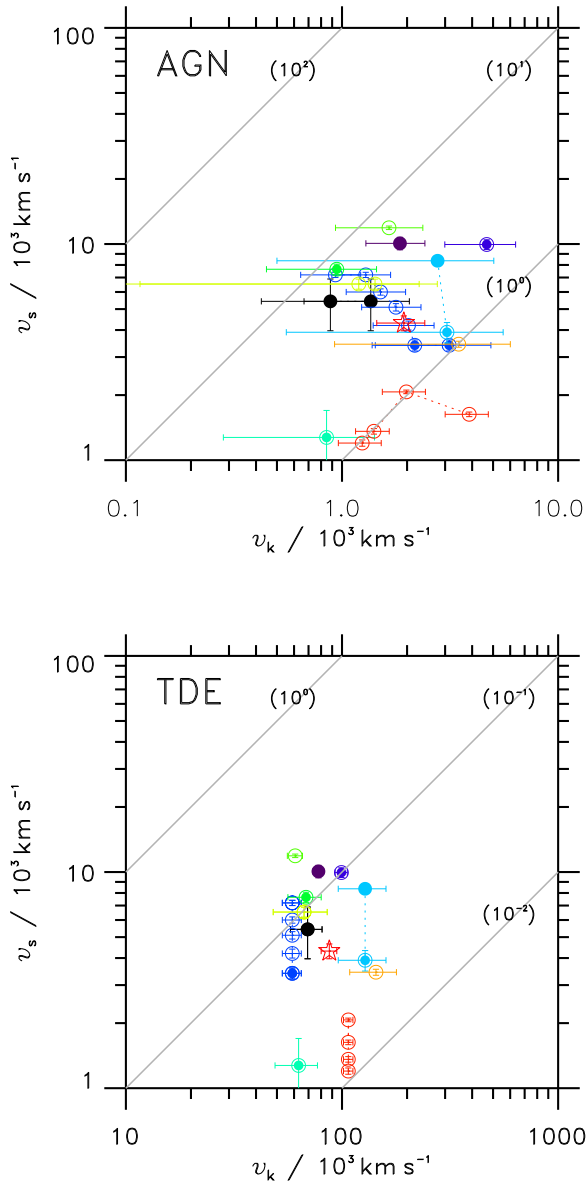


**Figure B1.** Comparison of observed velocity widths ( $v_s$ ) with expected Keplerian velocity ( $v_k$ ) estimated using scaling assumptions from AGN broad line regions (top) and TDE tidal radii (bottom). Guidelines mark the ratio  $v/v_k$  in powers of ten. Open circle symbols are events with H $\alpha$  emission; filled circles are events with He II emission; the starred event has broad absorption lines.

$$M_c = 4\pi R_c^2 \mu m_p N_H \Omega = \frac{L}{\bar{\epsilon} \Phi_H} \mu m_p N_H \Omega = \mu m_p \frac{L_\lambda}{I_\lambda} N_H, \quad (\text{C3})$$

where  $\mu$  is the mean molecular weight, and  $m_p$  is the proton mass. We can either make a fiducial assumption about the covering factor (e.g.  $\Omega = 0.1$ ), or we can calculate a self-consistent value if both the line luminosity and continuum luminosity are known,

$$\Omega = \frac{L_\lambda \bar{\epsilon} \Phi_H}{L I_\lambda}. \quad (\text{C4})$$

In practice,  $\Phi_H$  is a user-chosen runtime parameter;  $\bar{\epsilon}$  is a constant for each SED;  $I_\lambda$  is output from CLOUDY for given  $(N_H, n_H, \Phi_H)$ ;  $L_\lambda$  is the observed line luminosity; and the total luminosity  $L$  is observationally inferred. Thus we assemble cubes of results in the  $(N_H, n_H, \Phi_H)$  parameter cube, and give them quantitative interpretation in the empirical context of a specific TDE candidate. Imposing some common-sense conditions can whittle the possibilities, to leave a set of physically reasonable results.

- For self-consistency, the clouds must be outside the opaque photosphere of the central luminous source ( $R_c > R_o$ , where  $L_o = 4\pi R_o^2 \sigma T_o^4$  for a blackbody sphere).
- Clouds can't cover more than the whole source ( $\Omega < 1$ ).
- The He II/H $\alpha$  line ratio and the respective equivalent widths can be checked for consistency with observations.

Before interpreting the scale-independent CLOUDY results to model a particular TDE candidate event, a minority of the numerical output requires filtering for artifacts. For the hotter blackbody scenarios, a numerical instability sometimes occurs near the far end of the spatial grid, regardless of the total column density. These incidents cause CLOUDY to report global non-convergence (which might have been the numerical problem reported by [Strubbe & Murray 2015](#)). On close inspection, the majority of the profile is however stable. We retain these good sections, and excise the final 0.2 dex in  $N_H$ , and any cells where the He II intensity rises with a logarithmic gradient greater than 2. After this initial filtering, a smaller minority of numerical spikes remain; but their sensitivity to resolution proves their spuriousness. These glitches occur at uninterestingly low  $N_H$ , in configurations where the ionization parameter is low ( $U < 0.03$ ). From the  $10^6$  K and  $10^7$  K blackbody SEDs, we exclude models with  $U < 0.03$  ( $\Phi_H/n_H < 10^9$  cm s $^{-1}$ ). Since we accumulated three cubes of results at different final  $N_H$  for every hypothetical SED, we have enough redundant and overlapping calculations to leave a finely sampled combined cube after filtering.

The three-parameter cube of photoionization states in  $(N_H, n_H, \Phi_H)$  is conventionally visualized in terms of cross-sections: the constant- $N_H$  flux-density planes (e.g. [Korista & Goad 2004](#)). For our purposes, in evaluating the possible conditions surrounding UV/O nuclear transients, it is more useful to project the non-linear surfaces that maximise the ratio  $w$  of the He II to H $\alpha$  line intensities, consistent with the observation of the significant minority of He-overbright events. Fig. C1 shows the results of coarse mapping of the local peak ratio for given  $(n_H, \Phi_H)$  pairs on a grid with 0.1dex steps on each axis. Results of two blackbody light-echo model SEDs are shown. Line ratios (top-left panels) are effectively a projection down along the  $N_H$  (vertical) axis, showing the inclined ‘sausage’ of He-overbright states. The lower two panels show the equivalent widths of the two important lines, in the  $N_H$  conditions that gave the peak line ratio. The top-right panels show the  $N_H$  values that gave each peak line ratio. The He-overbright states appear to require column densities near the maximum values we explored. Echo models assume that the clouds were photoionized by an early, hard flash from a compact, hot source at the indicated blackbody temperature. We assume that the observed  $3 \times 10^4$  K UV/O continuum represents the later condition of the photosphere of an adiabatically expanding, spheroidal, radiation-dominated explosion. The effect of the

light-echo correction – early hard photoionization source superimposed on a later cooled continuum, according to the light crossing time – is to lower the equivalent widths.

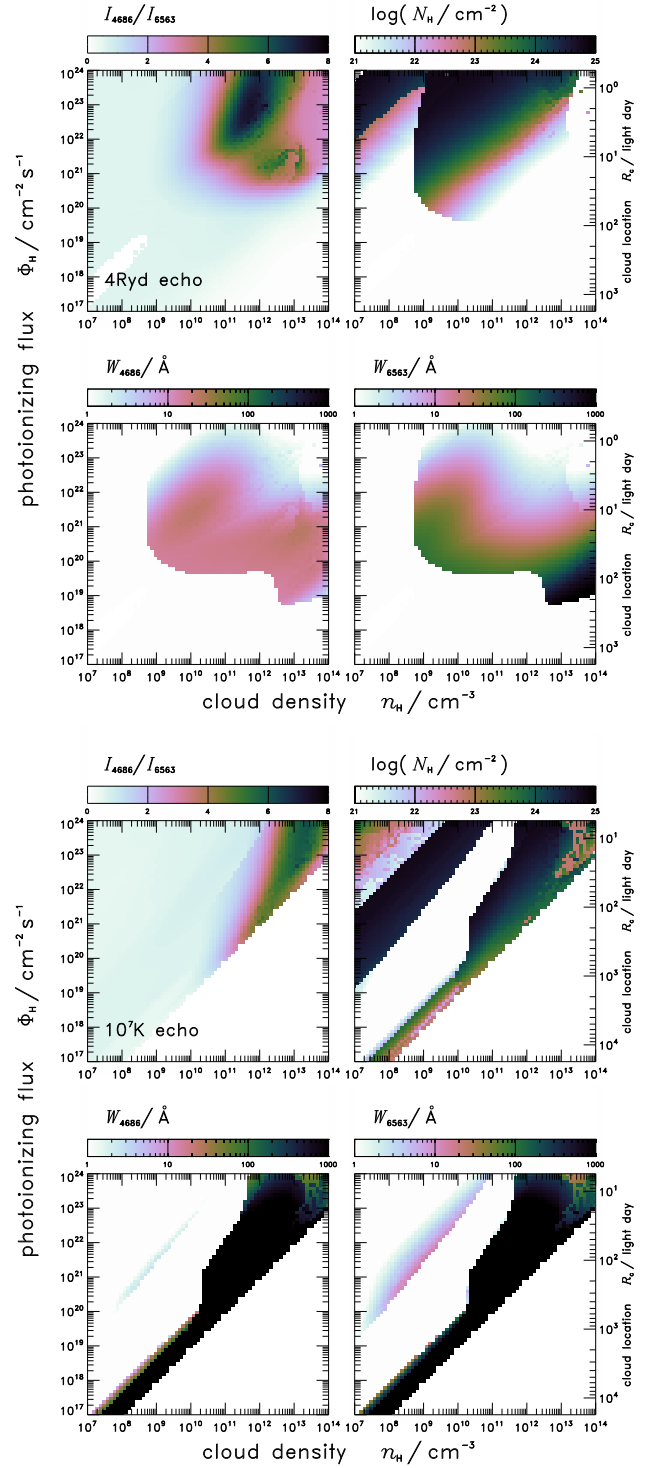


**Figure C1.** Conditions where  $N_{\text{H}}$  maximises the He II(4686Å) to Hα(6563Å) intensity ratio, at given  $(n_{\text{H}}, \Phi_{\text{H}})$ . The rows show the effect of blackbody SEDs except that the equivalent widths derive from continuum estimates in a ‘light echo’ model. Here we assume that the currently visible continuum is a blackbody of  $T_2 = 3 \times 10^4\text{K}$ , and the earlier flash illuminating the clouds is a 4Ryd or  $10^7\text{K}$  blackbody (top and bottom blocks respectively).